

D-A058 491

DAYTON UNIV OHIO RESEARCH INST
FINITE ELEMENT METHOD FOR THE FINITE-DISPLACEMENT ANALYSIS OF S--ETC(U)
APR 78 R A BROCKMAN, F K BOGNER

F/G 13/13

F33615-75-C-3009

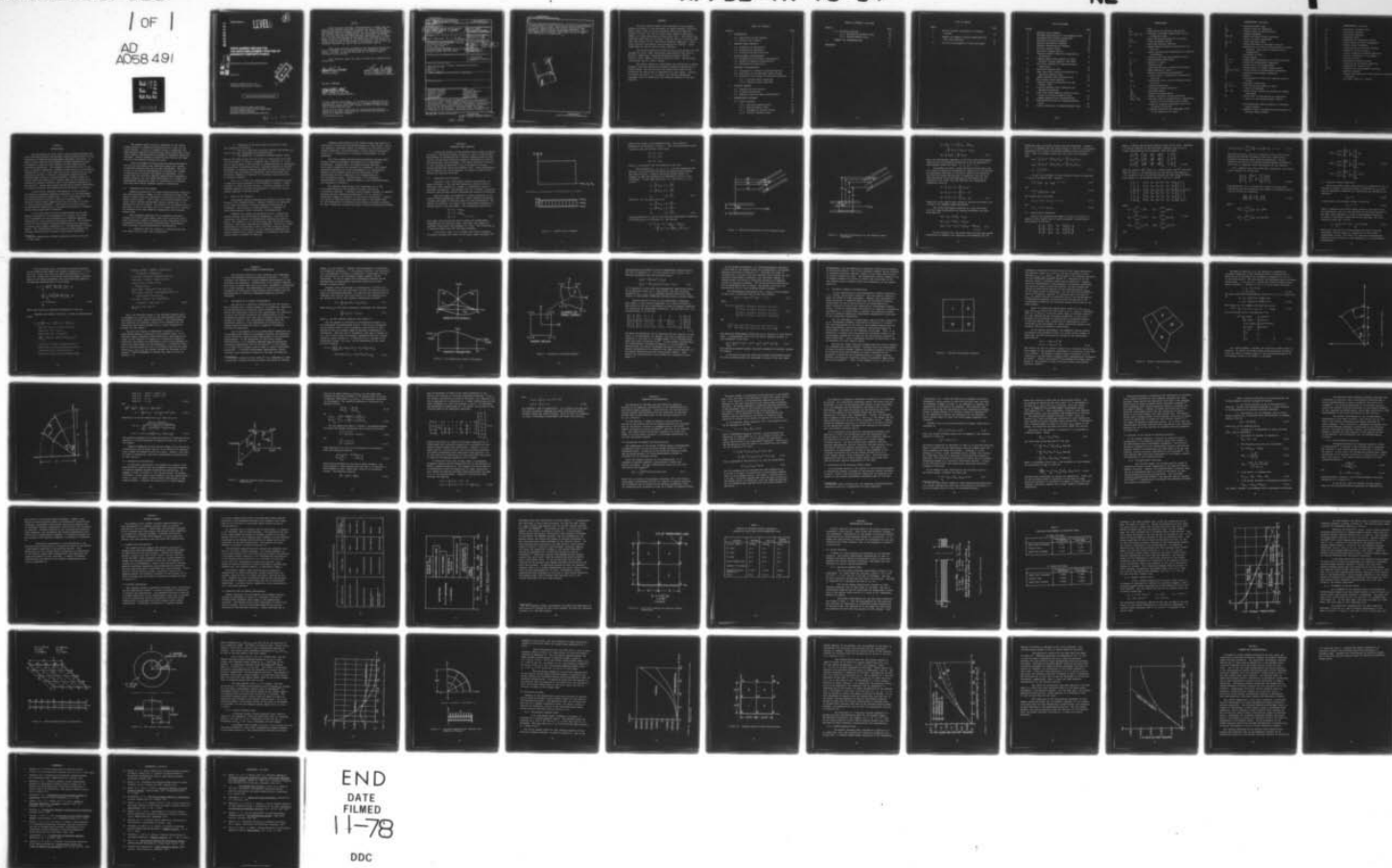
UNCLASSIFIED

AFFDL-TR-78-14

NL

/ OF /

AD
A058 491



END
DATE
FILMED
11-78
DDC

ADA058491

AFFDL-TR-78-14

LEVEL II

P.S.

**FINITE ELEMENT METHOD FOR
THE FINITE-DISPLACEMENT ANALYSIS OF
SANDWICH COMPOSITE PANELS**

AD No. _____
DDC FILE COPY

UNIVERSITY OF DAYTON RESEARCH INSTITUTE

APRIL 1978

TECHNICAL REPORT AFFDL-TR-78-14
Final Report for Period July 1975 - July 1976

DDC
SEP 11 1978
F

Approved for public release; distribution unlimited.

AIR FORCE FLIGHT DYNAMICS LABORATORY
AIR FORCE WRIGHT AERONAUTICAL LABORATORIES
AIR FORCE SYSTEMS COMMAND
WRIGHT-PATTERSON AIR FORCE BASE, OHIO 45433

78 15 08 074

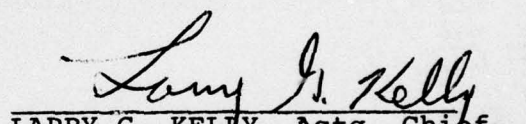
NOTICE

When Government drawings, specifications, or other data are used for any purpose other than in connection with a definitely related Government procurement operation, the United States Government thereby incurs no responsibility nor any obligation whatsoever; and the fact that the government may have formulated, furnished, or in any way supplied the said drawings, specifications, or other data, is not to be regarded by implication or otherwise as in any manner licensing the holder or any other person or corporation, or conveying any rights or permission to manufacture, use, or sell any patented invention that may in any way be related thereto.

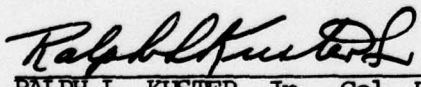
This report has been reviewed by the Information Office (OI) and is releasable to the National Technical Information Service (NTIS). At NTIS, it will be available to the general public, including foreign nations.

This technical report has been reviewed and is approved for publication.


HAROLD C. CROOP
Project Engineer


LARRY G. KELLY, Actg. Chief
Structural Concepts Branch
Structural Mechanics Division

FOR THE COMMANDER


RALPH L. KUSTER, Jr., Col, USAF
Chief, Structural Mechanics Division

"If your address has changed, if you wish to be removed from our mailing list, or if the addressee is no longer employed by your organization please notify FBS, W-PAFB, OH 45433 to help us maintain a current mailing list".

Copies of this report should not be returned unless return is required by security considerations, contractual obligations, or notice on a specific document.

UNCLASSIFIED

SECURITY CLASSIFICATION OF THIS PAGE (When Data Entered)

1. REPORT DOCUMENTATION PAGE		READ INSTRUCTIONS BEFORE COMPLETING FORM	
REPORT NUMBER AFFDL-TR-78-14	2. GOVT ACCESSION NO.	3. RECIPIENT'S CATALOG NUMBER	
4. TITLE (and Subtitle) FINITE ELEMENT METHOD FOR THE FINITE- DISPLACEMENT ANALYSIS OF SANDWICH COMPOSITE PANELS,		5. TYPE OF REPORT & PERIOD COVERED Final Report, July 1975-July 1976	
6. AUTHOR(s) Robert A. Brockman Fred K. Bogner		7. CONTRACT OR GRANT NUMBER(s) F33615-75-C-3009 F33615-77-C-3075	
8. PERFORMING ORGANIZATION NAME AND ADDRESS University of Dayton Research Institute 300 College Park Avenue Dayton, Ohio 45469 105 400		9. PROGRAM ELEMENT, PROJECT, TASK AREA & WORK UNIT NUMBERS 1368/02/17 241/03/11 1702, 03	
10. CONTROLLING OFFICE NAME AND ADDRESS Air Force Flight Dynamics Laboratory (FBS) Wright-Patterson AFB, Ohio 45433		11. REPORT DATE April 1978	
12. MONITORING AGENCY NAME & ADDRESS (if different from Controlling Office)		13. SECURITY CLASS. (of this report) UNCLASSIFIED	
14. DISTRIBUTION STATEMENT (of this Report) Approved for public release; distribution unlimited. 12 85 p.		15a. DECLASSIFICATION/DOWNGRADING SCHEDULE	
17. DISTRIBUTION STATEMENT (of the abstract entered in Block 20, if different from Report) 62201F			
18. SUPPLEMENTARY NOTES			
19. KEY WORDS (Continue on reverse side if necessary and identify by block number) structural analysis composite structure geometric linearity laminated plates finite element isoparametric Coon's patch conjugate gradients sandwich panel Hermite bicubic curved boundary variable metric			
20. ABSTRACT (Continue on reverse side if necessary and identify by block number) A finite element method is presented for the large deflection analysis of flat, layered sandwich panels having arbitrarily-shaped boundaries. Fully compatible isoparametric elements based upon Hermite bicubic interpolation are formulated, and requirements for the satisfaction of both displacement and slope compatibility are discussed. As special cases, the analysis can be applied to thin laminated plates and multicore sandwich, as			

DD FORM 1 JAN 73 1473 EDITION OF 1 NOV 65 IS OBSOLETE

UNCLASSIFIED

SECURITY CLASSIFICATION OF THIS PAGE (When Data Entered)

105 400

xlt

UNCLASSIFIED

SECURITY CLASSIFICATION OF THIS PAGE(When Data Entered)

20.

well as elastically-supported plates. Solutions for geometrically nonlinear behavior are obtained by either the conjugate gradient or variable metric method. Applications presented include rectangular, skewed, annular and circular geometries. The analysis is shown to maintain displacement and stress accuracy for elements having extremely large aspect ratios, or edges which degenerate to a single point.

ACCESSION	Section <input checked="" type="checkbox"/>
NTIS	Section <input type="checkbox"/>
DDC	
UNANIM	
JSTH	
BY	DISTRIBUTION/AVAILABILITY CODES
Dist.	SPECIAL
A	

UNCLASSIFIED

SECURITY CLASSIFICATION OF THIS PAGE(When Data Entered)

FOREWORD

The work reported herein was performed by the Aerospace Mechanics Division of the University of Dayton Research Institute, Dayton, Ohio, under Air Force Contracts F33615-75-C-3009 and F33615-77-C-3075, for the Air Force Flight Dynamics Laboratory (AFFDL) at Wright-Patterson Air Force Base, Ohio. This effort was conducted under Task 02 of Project 1368 and Task 03 of Project 2401 under the general title, "Structural Sandwich Composites." Technical direction and support was provided by Mr. Harold C. Croop (AFFDL/FBS) as the Air Force Project Engineer.

The work described was conducted during the period July 1975 through July 1976, under the general supervision of Mr. Dale H. Whitford, Supervisor, Aerospace Mechanics Division, and Mr. George J. Roth, Leader, Structural Analysis Group. The principal investigator was Dr. Fred K. Bogner.

The author gratefully acknowledges the University of Dayton Research Institute library for providing reference materials in a timely manner, and the clerical and Graphic Arts staff of the University for their help in preparation of this report. Particular thanks are due Dr. F. K. Bogner for numerous suggestions regarding both the theoretical and numerical aspects of the work reported.

TABLE OF CONTENTS

Section	Page
1 INTRODUCTION	1
1.1 Description of the Problem	2
1.2 Scope of the Analysis	3
2 SANDWICH PANEL ANALYSIS	5
2.1 Kinematics of Deformation	5
2.2 Stress-Strain Equations	11
2.3 Potential Energy Formulation	14
3 FINITE ELEMENT DISCRETIZATION	17
3.1 Interpolation of Element Displacements	17
3.2 Parametric Mapping Considerations	23
3.3 Compatibility Constraints	30
4 NUMERICAL CONSIDERATIONS	35
4.1 Calculation of Element Stiffness Matrices	35
4.2 Evaluation of the Nonlinear Strain Energy	37
4.3 Solution of the System of Nonlinear Equations	40
4.3.1 Fletcher-Powell Algorithm	40
4.3.2 Fletcher-Reeves Algorithm	42
5 COMPUTER PROGRAM	44
5.1 Program Size and Capacity	44
5.2 Program Organization	44
5.3 Computing Time and Memory Requirements	45
6 DEMONSTRATION PROBLEMS	51
6.1 Linear Analyses	51
6.1.1 Multicore Sandwich Beam	51
6.1.2 Skewed Sandwich Plate	54
6.1.3 Axisymmetric Annular Plates	56
6.1.4 Circular Sandwich Panel	59

TABLE OF CONTENTS, concluded

Section	Page
6.2 Nonlinear Analyses	62
6.2.1 Rectangular Sandwich Plate	62
6.2.2 Skewed Sandwich Plate	65
7 SUMMARY AND RECOMMENDATIONS	69
REFERENCES	71

LIST OF TABLES

TABLE		PAGE
1	Solution Methods Implemented in Computer Program	46
2	Results of Computer Program Comparisons for Flat Plate Analysis	50
3	Free End Displacements of Multicore Beams	53

LIST OF FIGURES

FIGURE		PAGE
1	Sandwich Panel Geometry	6
2	Deformed Configuration of the Sandwich Panel	8
3	One-Dimensional Hermite Polynomials	19
4	Parametric Coordinate Mapping	20
5	Adjacent Rectangular Elements	24
6	Adjacent Nonrectangular Elements	26
7	Circular Element Sector	28
8	Elliptical Element Sector	29
9	Adjacent Elements Requiring Compatibility Constraints	31
10	Computer Memory Requirements for Major Computer Program Segments (CDC 6600)	47
11	Flat Plate Problem for Computer Program Comparisons	49
12	Multicore Sandwich Beam	52
13	Lower Face Sheet Stress Distributions in Multicore Sandwich Beam	55
14	Skewed Sandwich Panel Discretization	57
15	Thin Annular Sheet Geometry	58
16	Computed Stress Distributions for Thin Annular Plate	60
17	Circular Sandwich Panel Modelled with Degenerate Elements	61
18	Lower Face Sheet Membrane Stress Distribu- tions in Circular Sandwich Plate	63
19	Clamped Sandwich Plate Discretization	64
20	Load-Deflection Path for Clamped Sandwich Plate	66
21	Central Deflection of Skewed Sandwich Panel	68

NOMENCLATURE

A	- area
A, B	- identifiers for specific node points
A_{ij}, B_{ij}, D_{ij}	- resultant stiffness coefficients for an orthotropic layer
a, b	- major and minor semiaxes of an ellipse
a, b, c, d	- fixed coordinate values
C	- arbitrary material constant
C^n	- symbol denoting degree of continuity of a function
C_{ij}	- lamina stress-strain coefficients in material coordinates
c	- subscript denoting the sandwich core(s)
c_1, c_2	- undetermined coefficients
E_i	- modulus of layer i
F	- function value
f	- subscript denoting a sandwich face sheet
G_i	- shear modulus of layer i
H_{ij}	- Hermite interpolation polynomials
$\{H\}$	- column vector of polynomial interpolation functions
$[H]_i$	- approximate metric used in Fletcher-Powell solution
I, II	- element identifiers
k	- individual lamina identifier
$[K]$	- stiffness matrix
$[K]_e$	- element stiffness matrix
M_i, N_i	- moment and direct stress resultants
$[M]_i, [N]_i$	- matrices used in constructing an approximate metric in the Fletcher-Powell method
n	- number of Gaussian quadrature points per coordinate direction
o	- subscript denoting the undeformed state, or the midplane of a layer

NOMENCLATURE, continued

p	- applied pressure load
p_i	- surface traction components
$\{p\}$	- column vector of applied forces
Q	- loading parameter
$\{Q\}, \{R\}$	- moment and shear stress resultants
r	- radius in polar coordinates
r_i, r_o	- inner and outer radii
\vec{s}_i	- search direction in nonlinear solution
T	- denotes typical term in strain energy or energy gradient. Also used to indicate matrix transposition
t_i	- thickness of layer i
U	- strain energy
U, V, W	- displacement components at an arbitrary point
u, v, w	- midsurface displacement components
$\{U\}$	- column vector of displacements
$\{U_E\}$	- column vector of element displacements
$\{U_i\}, \{V_i\}, \{W_i\}$	- column vectors of displacement components
$\{u\}$	- Cartesian displacement components
V	- volume
W	- work potential function for applied external forces
x, y, z	- Cartesian coordinates
x_i, y_i, z_i	- local coordinate system at layer i
\vec{X}	- a vector of unknowns
$\{X\}, \{Y\}$	- column vectors containing geometrical mapping parameters
\vec{Y}_i	- vector used in constructing an approximate metric in the Fletcher-Powell method
α	- one-dimensional search parameter in Fletcher-Powell method
β_i	- parameter used in determining step direction in Fletcher-Powell method

NOMENCLATURE, concluded

γ_{ij}	- components of shear strain
Δ	- coordinate increment
δ	- variational operator
δ_{ij}	- Kronecker delta
ϵ_i	- components of extensional strain
$\{\epsilon\}$	- column vector of strain components
θ	- angular polar coordinate
$\{\kappa\}$	- column vector of curvature changes
ν_i	- Poisson's ratio of layer i
ξ_i	- natural coordinate interval endpoints
ξ, η	- natural coordinates of an element
π_p	- potential energy
σ_i	- components of direct stress
$\{\sigma\}$	- column vector of stress components
τ_{ij}	- components of shear stress
ϕ, ψ, χ	- sandwich core displacement functions
∇	- gradient operator
,	- denotes differentiation with respect to parameter following
$ \quad $	- Euclidean length of a vector

SECTION 1

INTRODUCTION

The development of light weight, high strength advanced composite materials affords the designer numerous possibilities for the production of improved high-performance aerospace structures. In order to fully exploit this progress, analysis capabilities must be expanded to keep pace with advances in both materials and fabrication technology. This comment is particularly true in the case of sandwich composites. Sandwich construction is an attractive alternative to other, more common structural configurations, since substantial benefit in terms of load-carrying capacity can be obtained under little or no weight penalty. However, modes of failure which are unheard of in simpler types of construction are possible in sandwich structures due to the inherent complexity of the geometry. Design and analysis methods which predict these modes of failure accurately and economically are therefore a necessity.

A particularly important consideration in the effective utilization of sandwich composite construction is the development of nonlinear analysis capabilities. It is a well-known fact that the shear flexibility which is typical of sandwich core materials places severe restrictions upon the range of validity of linear analysis methods^{1*}. Linearization has been shown to be particularly restrictive in the stability analysis of sandwich shells having significant curvature².

It is clear that the finite element method is the most promising approach to the development of analysis tools which will be adequate for the consideration of sandwich composite structures of a very practical and general nature. The piecewise nature of finite element representations permits the treatment of complex and irregular geometries in a straightforward, unified manner. The consideration of very general loading systems and boundary conditions also presents no particular difficulty.

* Numerical superscripts indicate references listed at the end of the report.

The present report outlines a procedure for the finite element analysis of sandwich structures by both linear and non-linear methods. A theory of sandwich plates is presented, and some important aspects of discretization using higher-order (cubic) finite element representations in parametric coordinate space are discussed. Several examples illustrating the accuracy and flexibility of the numerical analysis are given.

Since the sandwich structure analysis system described is not yet fully developed, many limitations remain and a number of desirable features have not yet been implemented. The limitations of the existing methodology are discussed and a number of suggestions for further development are mentioned. It is thought that the analytical approach adopted herein represents a useful foundation for the further development of a reliable and comprehensive mathematical model for the analysis of practical structures which employ sandwich composite construction.

1.1 Description of the Problem

Sandwich construction is a type of built-up panel configuration characterized by a number of thin, high-modulus layers (face sheets or skins) which are separated and stabilized by thicker, low-modulus layers (cores). Such a panel can be made extremely lightweight, while offering considerable bending rigidity due to the separation of the face sheets. The function of the sandwich core is analogous to that of the shear web of an I-beam section in coupling the response of the face sheets by transferring shear stresses between them.

While sandwich composites are an extremely attractive concept due to their light weight, their use in practical structures introduces a number of possible failure modes which are not encountered in other structural configurations. Specifically, these additional failure mechanisms are attributed to:

1. weakness of the core layer(s) in comparison with the face sheets, both in shear and in compression

2. inadequacy of the face sheets for resisting loads near fasteners and inserts
3. lack of a continuous interface between face sheets and core in cellular (honeycomb) core constructions
4. the possibility of defective bonding between layers.

Each of the above properties give rise to a particular local mode of failure which is unique to sandwich type construction. Since each of these types of failure must be considered both in formulating and qualifying a particular design, extensive analysis is required. Furthermore, a separate checking procedure for each possible type of failure may not always be sufficient, particularly when the structural component in question is to undergo large deflections or inelastic behavior.

Thus, it is clear that sandwich composite materials present a number of unique problems for the designer or analyst. Proper treatment of these problems requires a detailed analysis of the sandwich geometry and state of deformation, to which the finite element approach is ideally suited.

1.2 Scope of the Analysis

The present analysis addresses the problem of static deformation of flat sandwich panels. Material behavior is restricted to be linear and elastic, although geometric nonlinearity is considered. The analysis is thus applicable to problems of large displacements, elastic buckling, and postbuckling.

Sandwich face sheets are idealized as thin, layered composites obeying the Love-Kirchhoff assumptions. Isotropic and orthotropic thin plates can therefore be considered as special cases. The sandwich is of the anti-plane type (non-direct stress carrying), with normal deformations considered. The finite element discretization is performed in such a way that multicore panels, "half-sandwich" constructions, or thin laminated composites are easily considered by stacking elements or eliminating individual layers within an element as required.

External loads applied to the sandwich panel may consist of concentrated forces and distributed pressure or body forces. Due to the numerical integration which is necessary for calculation of the element properties, the specification of more complex distributed forces (i.e., hydrostatic or sinusoidal distributions) is also permitted.

The finite element discretization presented is based upon a Hermite bicubic displacement approximation in isoparametric coordinates. Skewed panels, or sandwich having arbitrary curvilinear boundaries can therefore be considered. The method described represents the first development of an isoparametric sandwich finite element which has the properties of both completeness and full compatibility of displacements as well as bending slopes. Considerations in the parametric representation of finite element geometry in the undeformed state are discussed in Section 3.

The research reported here also represents one of the first applications of the parametric bicubic formulation to nonlinear problems. A similar finite element treatment of sandwich analysis has been presented by Monforton³, but is limited to rectangular shapes in Cartesian or cylindrical coordinates. Significant gains in efficiency have also been made in the present work for the computation of nonlinear strain energy and energy gradients for use in numerical solutions by direct function minimization methods.

SECTION 2

SANDWICH PANEL ANALYSIS

A brief description of the sandwich theory which is used as a basis for the finite element analysis is given in this section. The geometry of deformation for a typical sandwich panel is discussed, and the total potential energy is formulated in terms of the displacement field unknowns. The theory presented is similar to that outlined by Monforton³, but is extended to include normal deformations within the sandwich core. Large displacements are considered, but the development is limited to small elastic strains and moderate rotations.

2.1 Kinematics of Deformation

Consider a flat, three-layer sandwich construction, as shown in Figure 1. The two face sheets are taken to be thin laminates, each composed of a number of orthotropic layers of arbitrary orientation. The sandwich core is a thicker, relatively flexible layer having constant thickness and material orientation.

Each face sheet is considered to deform according to the Love-Kirchhoff assumptions; that is, linear filaments originally straight and normal to the face remain so after deformation, and undergo no extension. In terms of the displacement variables at a general point in the face sheet, this assumption implies that

$$\begin{aligned}U_f &= u_f - z_f w_{f,x} \\V_f &= v_f - z_f w_{f,y} \\W_f &= w_f \quad ; f = 1, 2.\end{aligned}\tag{2.1}$$

Here upper case letters are used to denote the displacement components at any arbitrary point, and lower case symbols to represent those within the midplane of a face. The coordinate z_f is measured upward from the face sheet midplane.

In the core layer, it is assumed that linear filaments originally straight and normal to the layer remain straight, but

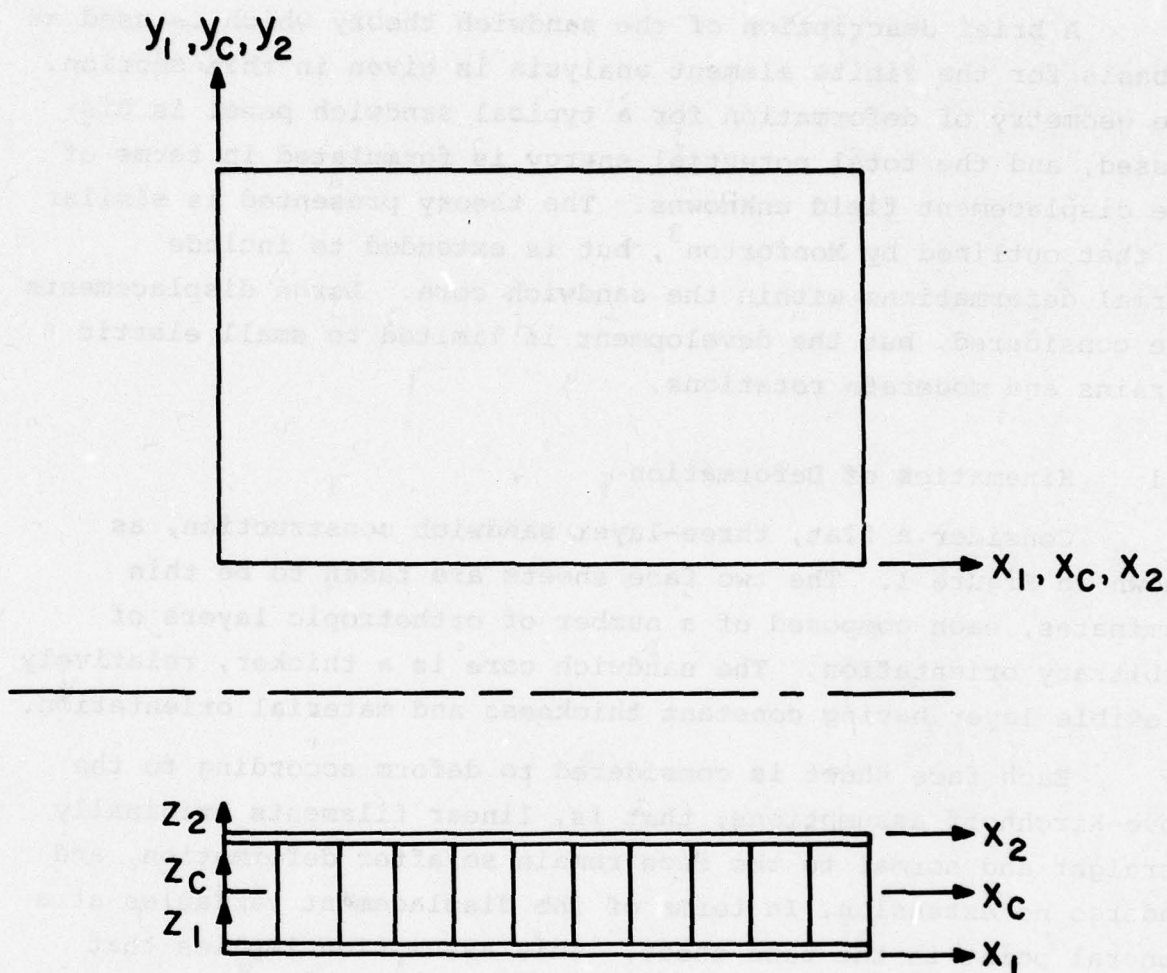


Figure 1. Sandwich Panel Geometry.

need not be normal to the deformed layer. This state of deformation is pictured in Figure 2. The core displacement state therefore takes the general linear form

$$\begin{aligned}U_c &= u_c + z_c \phi \\V_c &= v_c + z_c \psi \\W_c &= w_c + z_c \chi\end{aligned}\tag{2.2}$$

where z_c is measured from the midplane of the core.

The parameters $u_c, v_c, w_c, \phi, \psi, \chi$ can be eliminated from Equation 2.2 by enforcing continuity of displacements between the faces and core. Perfect continuity between layers is assumed, so that the possibility of debonding failure is not considered. At the lower bond line, $z_1 = t_1/2$ and $z_c = -t_c/2$ so that

$$\begin{aligned}u_1 - \frac{t_1}{2} w_{1,x} &= u_c - \frac{t_c}{2} \phi \\v_1 - \frac{t_1}{2} w_{1,y} &= v_c - \frac{t_c}{2} \psi \\w_1 &= w_c - \frac{t_c}{2} \chi.\end{aligned}\tag{2.3}$$

Similarly, for the upper bond line,

$$\begin{aligned}u_2 + \frac{t_2}{2} w_{2,x} &= u_c + \frac{t_c}{2} \phi \\v_2 + \frac{t_2}{2} w_{2,y} &= v_c + \frac{t_c}{2} \psi \\w_2 &= w_c + \frac{t_c}{2} \chi.\end{aligned}\tag{2.4}$$

Solving Equations 2.3 and 2.4 for the core displacement parameters and substituting in Equations 2.2, one obtains

$$\begin{aligned}U_c &= \frac{1}{2} (u_2 + u_1 + t_2 w_{2,x} - t_1 w_{1,x}) \\&\quad + \frac{z_c}{t_c} (u_2 - u_1 + \frac{t_2}{2} w_{2,x} + \frac{t_1}{2} w_{1,x})\end{aligned}$$

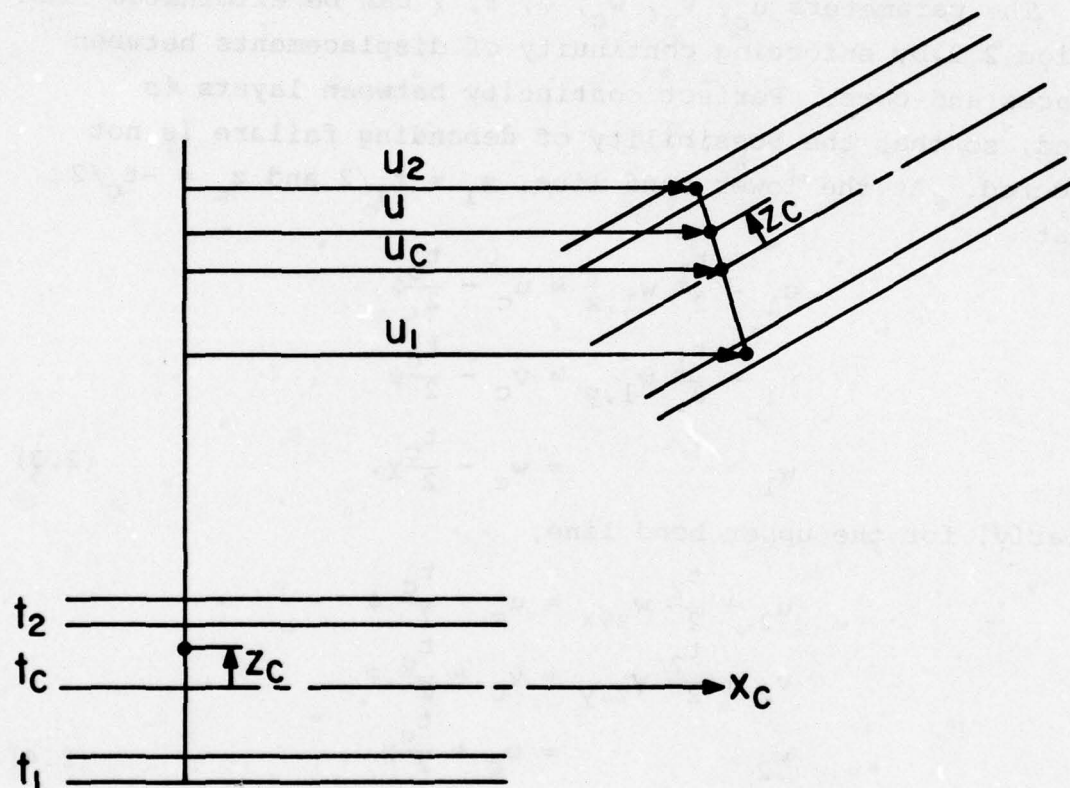


Figure 2. Deformed Configuration of the Sandwich Panel.

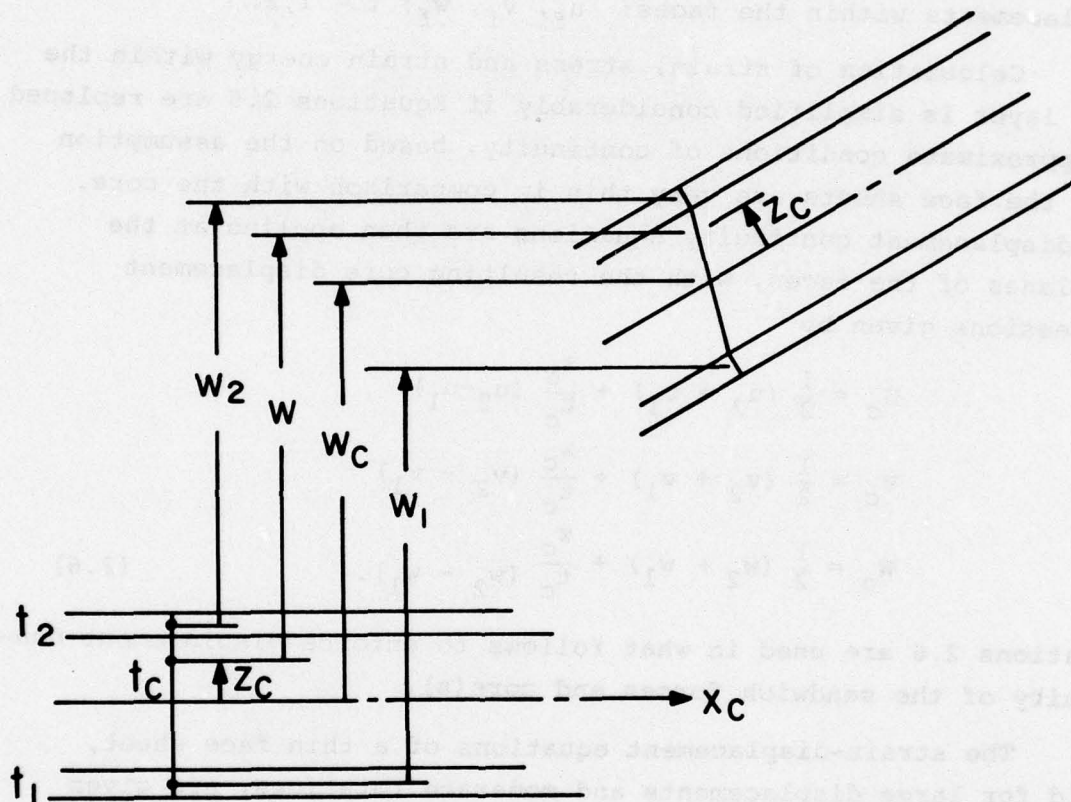


Figure 2. Deformed Configuration of the Sandwich Panel (concluded).

$$\begin{aligned}
V_c &= \frac{1}{2}(v_2 + v_1 + \frac{t_2}{2} w_{2,x} - \frac{t_1}{2} w_{1,x}) \\
&\quad + \frac{z_c}{t_c} (v_2 - v_1 + t_2 w_{2,x} + t_1 w_{1,x}) \\
W_c &= \frac{1}{2} (w_2 + w_1) + \frac{z_c}{t_c} (w_2 - w_1)
\end{aligned} \tag{2.5}$$

Thus, the displacement components of any point within the sandwich faces or core are completely determined by the six components of displacements within the faces: u_f, v_f, w_f ; $f = 1, 2$.

Calculation of strain, stress and strain energy within the core layer is simplified considerably if Equations 2.5 are replaced by approximate conditions of continuity, based on the assumption that the face sheets are very thin in comparison with the core. The displacement continuity equations are then applied at the midplanes of the faces, with the resulting core displacement expressions given by

$$\begin{aligned}
U_c &= \frac{1}{2} (u_2 + u_1) + \frac{z_c}{t_c} (u_2 - u_1) \\
V_c &= \frac{1}{2} (v_2 + v_1) + \frac{z_c}{t_c} (v_2 - v_1) \\
W_c &= \frac{1}{2} (w_2 + w_1) + \frac{z_c}{t_c} (w_2 - w_1).
\end{aligned} \tag{2.6}$$

Equations 2.6 are used in what follows to enforce displacement continuity of the sandwich forces and core(s).

The strain-displacement equations of a thin face sheet, valid for large displacements and moderate rotations, are given by Novozhilov⁴:

$$\begin{aligned}
\epsilon_{xf} &= u_{f,x} + \frac{1}{2} w_{f,x}^2 - z_f w_{f,xx} \\
\epsilon_{yf} &= u_{f,y} + \frac{1}{2} w_{f,y}^2 - z_f w_{f,yy} \\
\gamma_{xyf} &= u_{f,y} + v_{f,x} + w_{f,x} w_{f,y} - 2z_f w_{f,xy};
\end{aligned} \tag{2.7}$$

$f = 1, 2.$

For the sandwich core, the strain energy arising from inplane deformations is assumed to be negligible, and therefore only the

transverse shear and normal strains need be considered. Furthermore, it is assumed that the strain energy of the core is adequately represented by a linear relationship between strain and displacement. Thus, the strains within the core layer are calculated from

$$\begin{aligned}\gamma_{xzc} &= \frac{1}{t_c} (u_2 - u_1) + \frac{1}{2} (w_{2,x} + w_{1,x}) + \frac{z_c}{t_c} (w_{2,x} - w_{1,x}) \\ \gamma_{yzc} &= \frac{1}{t_c} (v_2 - v_1) + \frac{1}{2} (w_{2,y} + w_{1,y}) + \frac{z_c}{t_c} (w_{2,y} - w_{1,y}) \\ \epsilon_{zc} &= \frac{1}{t_c} (w_2 - w_1)\end{aligned}\quad (2.8)$$

It will be convenient in what follows to refer to Equations 2.7 and 2.8 in matrix form. Letting

$$\{\epsilon\}_f^T = \begin{bmatrix} \epsilon_{xf} & \epsilon_{yf} & \gamma_{xyf} \end{bmatrix} ; f = 1, 2 \quad (2.9)$$

and

$$\{\epsilon\}_c^T = \begin{bmatrix} \gamma_{xzf} & \gamma_{yzf} & \epsilon_{zc} \end{bmatrix} , \quad (2.10)$$

the strains are of the form

$$\{\epsilon\}_f = \{\epsilon^0\}_f + z_f \{\kappa\}_f ; f = 1, 2 \quad (2.11)$$

and

$$\{\epsilon\}_c = \{\epsilon^0\}_c + z_c \{\kappa\}_c . \quad (2.12)$$

2.2 Stress-Strain Equations

Each of the sandwich face sheets is taken to consist of a number of thin layers, each of which possesses a stress-strain relationship of the form

$$\begin{Bmatrix} \sigma_1 \\ \sigma_2 \\ \tau_{12} \end{Bmatrix} = \begin{bmatrix} C_{11} & C_{12} & C_{16} \\ C_{12} & C_{22} & C_{26} \\ C_{16} & C_{26} & C_{66} \end{bmatrix} \begin{Bmatrix} \epsilon_1 \\ \epsilon_2 \\ \gamma_{12} \end{Bmatrix} \quad (2.13)$$

where 1,2 denote the principal material axes of the layer. Equation 2.13 can be referred to the structural reference axes x,y by a linear transformation of coordinates, with the result

$$\begin{Bmatrix} \sigma_x^{(k)} \\ \sigma_y^{(k)} \\ \tau_{xy}^{(k)} \end{Bmatrix}_f = \begin{bmatrix} Q_{11}^{(k)} & Q_{12}^{(k)} & Q_{16}^{(k)} \\ Q_{12}^{(k)} & Q_{22}^{(k)} & Q_{26}^{(k)} \\ Q_{16}^{(k)} & Q_{26}^{(k)} & Q_{66}^{(k)} \end{bmatrix}_f \begin{Bmatrix} \epsilon_x^{(k)} \\ \epsilon_y^{(k)} \\ \gamma_{xy}^{(k)} \end{Bmatrix}_f \quad (2.14)$$

Here the notation $\sigma_{xf}^{(k)}$ refers to a stress within the k^{th} individual layer of face f. By substituting for the strains from Equation 2.11, Equation 2.14 is integrated through the face sheet thickness with respect to the weighting factors 1 and z_f to yield⁵

$$\begin{Bmatrix} N_x \\ N_y \\ N_{xy} \\ -M_x \\ M_y \\ M_{xy} \end{Bmatrix}_f = \begin{bmatrix} A_{11} & A_{12} & A_{16} & B_{11} & B_{12} & B_{16} \\ A_{12} & A_{22} & A_{26} & B_{12} & B_{22} & B_{26} \\ A_{16} & A_{26} & A_{66} & B_{16} & B_{26} & B_{66} \\ B_{11} & B_{12} & B_{16} & D_{11} & D_{12} & D_{16} \\ B_{12} & B_{22} & B_{26} & D_{12} & D_{22} & D_{26} \\ B_{16} & B_{26} & B_{66} & D_{16} & D_{26} & D_{66} \end{bmatrix}_f \begin{Bmatrix} \epsilon_x \\ \epsilon_y \\ \gamma_{xy} \\ \kappa_x \\ \kappa_y \\ \kappa_{xy} \end{Bmatrix}_f \quad (2.15)$$

where

$$\begin{aligned} N_x &= \int_{-t_f/2}^{t_f/2} \sigma_x dz_f & M_x &= \int_{-t_f/2}^{t_f/2} \sigma_x z_f dz_f \\ N_y &= \int_{-t_f/2}^{t_f/2} \sigma_y dz_f & M_y &= \int_{-t_f/2}^{t_f/2} \sigma_y z_f dz_f \\ N_{xy} &= \int_{-t_f/2}^{t_f/2} \tau_{xy} dz_f & M_{xy} &= \int_{-t_f/2}^{t_f/2} \tau_{xy} z_f dz_f \end{aligned} \quad (2.16)$$

and

$$(A_{ij}, B_{ij}, D_{ij})_f = \int_{-t_f/2}^{t_f/2} Q_{ijf}^{(k)} (1, z_f, z_f^2) dz_f; \quad f = 1, 2 \quad (2.17)$$

The coefficients A_{ij} and D_{ij} in Equation 2.15 are the overall membrane and bending stiffness of the face, respectively, including extensional-shear coupling properties. The B_{ij} represent the effects of coupling between membrane and bending action due to asymmetry about the midplane of the laminate.

For a sandwich core with orthotropic properties, the stress-strain relation is of the form

$$\begin{Bmatrix} \tau_{xz} \\ \tau_{yz} \\ \sigma_z \end{Bmatrix}_c = \begin{bmatrix} G_{xz} & 0 & 0 \\ 0 & G_{yz} & 0 \\ 0 & 0 & E_z \end{bmatrix}_c \begin{Bmatrix} \gamma_{xz} \\ \gamma_{yz} \\ \epsilon_z \end{Bmatrix}_c \quad (2.18)$$

Using Equation 2.12 to evaluate the vector of strains, and integrating over the thickness with respect to weighting factors 1 and z_c yields the following

$$\begin{Bmatrix} Q \\ R \end{Bmatrix}_c = \begin{bmatrix} A & B \\ B & D \end{bmatrix}_c \begin{Bmatrix} \epsilon^o \\ \kappa \end{Bmatrix}_c \quad (2.19)$$

where

$$\begin{aligned} \{Q\}_c^T &= \int_{-t_c/2}^{t_c/2} [\tau_{xz} \quad \tau_{yz} \quad \sigma_z] dz_c \\ \{R\}_c^T &= \int_{-t_c/2}^{t_c/2} [\tau_{xz} \quad \tau_{yz} \quad \sigma_z] z_c dz_c \end{aligned} \quad (2.20)$$

and

$$\begin{aligned}
[A]_c &= \int_{-t_c/2}^{t_c/2} \begin{bmatrix} G_{xz} & 0 & 0 \\ 0 & G_{yz} & 0 \\ 0 & 0 & E_z \end{bmatrix} dz_c \\
[B]_c &= \int_{-t_c/2}^{t_c/2} \begin{bmatrix} G_{xz} & 0 & 0 \\ 0 & G_{yz} & 0 \\ 0 & 0 & E_z \end{bmatrix} z_c dz_c \\
[D]_c &= \int_{-t_c/2}^{t_c/2} \begin{bmatrix} G_{xz} & 0 & 0 \\ 0 & G_{yz} & 0 \\ 0 & 0 & E_z \end{bmatrix} z_c^2 dz_c
\end{aligned} \tag{2.21}$$

2.3 Potential Energy Formulation

Since the problem under consideration is conservative, it is possible to deduce a potential energy of deformation, π_p , such that the necessary conditions for equilibrium are defined by the condition⁶

$$\delta \pi_p = 0. \tag{2.22}$$

In particular, the potential energy is given by

$$\pi_p = U - W \tag{2.23}$$

where U represents the strain energy stored in the body due to its deformation, and W is the potential of the forces applied to the body, both expressed in terms of displacement functions. In terms of Lagrangian stress and strain functions, the total potential energy has the form

$$\pi_p = \iiint_{V_0} \frac{1}{2} \{\epsilon\}^T \{\sigma\} dV - \iint_{S_0^o} \{u\}^T \{P\} dA, \tag{2.24}$$

where S_0^o is the portion of the surface over which loads are prescribed, and the extent of integration is the initial (undeformed) volume. The vector $\{P\}$ consists of generalized external forces conjugate to the components $\{u\}$ of generalized displacement.

For the present case, the stress and strain functions in the sandwich face sheets are defined in Equations 2.7, 2.11, and 2.15; in the core, they are given by Equations 2.8, 2.12, and 2.19. Making use of the direct stress and moment resultant forms of the stress parameters, the total potential energy of the deformed sandwich panel is as follows:

$$\begin{aligned} \pi_p = & \iint_{A_c} \frac{1}{2} \left\{ \begin{matrix} \epsilon \\ \kappa \end{matrix} \right\}_c^T \left[\begin{matrix} A & I & B \\ B & I & D \end{matrix} \right]_c \left\{ \begin{matrix} \epsilon \\ \kappa \end{matrix} \right\}_c dA \\ & + \sum_{f=1}^2 \iint_{A_c} \frac{1}{2} \left\{ \begin{matrix} \epsilon \\ \kappa \end{matrix} \right\}_f^T \left[\begin{matrix} A & I & B \\ B & I & D \end{matrix} \right]_f \left\{ \begin{matrix} \epsilon \\ \kappa \end{matrix} \right\}_f dA \\ & - \iint_{S_o} \{u\}^T \{P\} dA, \end{aligned} \quad (2.25)$$

where the strains are defined by Equations 2.7 and 2.8.

Expanding the energy functional in terms of displacements gives

$$\begin{aligned} \pi_p = & \frac{1}{2} \iint_{A_c} \left[\frac{G_{xzc}}{t_c} (u_2 - u_1)^2 + \frac{G_{yzc}}{t_c} (v_2 - v_1)^2 + \frac{E_{zc}}{t_c} (w_2 - w_1)^2 \right. \\ & + G_{xzc} (u_2 - u_1) (w_{1,x} + w_{2,x}) + G_{yzc} (v_2 - v_1) (w_{1,y} + w_{2,y}) \\ & + \frac{1}{3} G_{xzc} t_c (w_{2,x}^2 + w_{1,x}^2 - w_{1,x} w_{2,x}) \\ & + \left. \frac{1}{3} G_{yzc} t_c (w_{2,y}^2 + w_{1,y}^2 - w_{1,y} w_{2,y}) \right] dA \\ & + \frac{1}{2} \sum_{f=1}^2 \iint_{A_f} \left\{ A_{11f} u_{f,x}^2 + A_{22f} v_{f,y}^2 + A_{66f} (u_{f,y} + v_{f,x})^2 \right. \\ & + 2A_{12f} u_{f,x} v_{f,y} + 2(A_{16f} u_{f,x} + A_{26f} v_{f,y}) (u_{f,y} + v_{f,x}) \\ & - 2 \left[B_{11f} u_{f,x} w_{f,xx} + B_{22f} v_{f,y} w_{f,yy} + 2B_{66f} w_{f,xy} (u_{f,y} + v_{f,x}) \right. \\ & + B_{12f} (v_{f,xx} + u_{f,xy}) + B_{16f} w_{f,xx} (u_{f,y} + v_{f,x}) \\ & \left. \left. + 2B_{16f} u_{f,x} w_{f,xy} + B_{26f} w_{f,yy} (u_{f,y} + v_{f,x}) + 2B_{26f} u_{f,y} w_{f,xy} \right] \right\} dA \end{aligned}$$

$$\begin{aligned}
& + D_{11f} w_{f,xx}^2 + D_{22f} w_{f,yy}^2 + 4D_{66f} w_{f,xy}^2 + 2D_{12f} w_{f,xx} w_{f,yy} \\
& + 4D_{16f} w_{f,xx} w_{f,xy} + 4D_{26f} w_{f,yy} w_{f,xy} \\
& + A_{11f} u_{f,x} w_{f,x}^2 + A_{22f} v_{f,y} w_{f,y}^2 + 2A_{66f} w_{f,x} w_{f,y} (u_{f,y} + v_{f,x}) \\
& + A_{12f} (u_{f,x} w_{f,y}^2 + v_{f,y} w_{f,x}^2) + A_{16f} w_{f,x}^2 (u_{f,y} + v_{f,x}) \\
& + 2A_{16f} u_{f,x} w_{f,x} w_{f,y} + A_{26f} w_{f,y}^2 (u_{f,y} + v_{f,x}) \\
& + 2A_{26f} v_{f,y} w_{f,x} w_{f,y} \\
& - \left[B_{11f} w_{f,xx} w_{f,x}^2 + B_{22f} w_{f,yy} w_{f,y}^2 + 4B_{66f} w_{f,x} w_{f,y} w_{f,xy} \right. \\
& + B_{12f} (w_{f,xx} w_{f,y}^2 + w_{f,yy} w_{f,x}^2) + 2B_{16f} (w_{f,xy} w_{f,x}^2 + w_{f,xx} w_{f,x} w_{f,y}) \\
& \left. + 2B_{26f} (w_{f,xy} w_{f,y}^2 + w_{f,yy} w_{f,x} w_{f,y}) \right] \\
& + \frac{1}{4} (A_{11f} w_{f,x}^4 + A_{22f} w_{f,y}^4) + (A_{66f} + \frac{1}{2} A_{12f}) w_{f,x}^2 w_{f,y}^2 \\
& + (A_{16f} w_{f,x}^3 w_{f,y} + A_{26f} w_{f,x} w_{f,y}^3) \} dA \\
& - \sum_{f=1}^2 \iint_{A_f^0} (p_x u_f + p_y v_f + p_z w_f) dA
\end{aligned} \tag{2.26}$$

Thus, the potential energy of the deformed sandwich panel is expressed as a function only of the displacements within the face sheets and their spatial derivatives. The displacements (and therefore the potential energy) of the sandwich core are obtained by what may be thought of as a linear interpolation between the face sheets.

The potential energy as formulated in Equation 2.26 is sufficiently general to describe a flat sandwich panel, of an arbitrary shape, undergoing large deflections, which may be due either to the intensity of loading or to buckling instability. Dissimilar face sheets are considered as well as any asymmetry of either face sheet about its own midsurface. It should be noted that in obtaining Equation 2.26 it is assumed that the core properties G_{xzc} , G_{yzc} , E_{zc} are uniform through the thickness of the sandwich. This corresponds to setting $[B]_c$ equal to zero in Equation 2.19.

SECTION 3

FINITE ELEMENT DISCRETIZATION

The potential energy of a flat sandwich panel undergoing finite displacements has been formulated in Section 2. In the following, the details of a finite element discretization of the structure are considered. Interpolation of the element displacement state is established using the natural (parametric) coordinates of a finite element. The enforcement of continuity of both displacements and transverse slopes between finite elements and the representation of arbitrary undeformed geometries are also discussed.

3.1 Interpolation of Element Displacements

The choice of a method of interpolation for the displacement variables over a single element is of fundamental importance in the formulation of structural finite elements. Not only should the displacement field be well-represented; the computation of strain and stress information by differentiation of the interpolation formula must also yield acceptable accuracy with a minimum of elements. For isoparametric elements where the undeformed geometry is also represented by interpolation, a careful choice of basis functions is essential to modeling accuracy and efficiency.

Due to the adoption of the Love-Kirchhoff assumptions for the sandwich face sheets in the present analysis, the potential energy functional contains second derivatives of the transverse displacements. In the application of the finite element discretization, it is therefore required that the approximate transverse displacement field be of class C^{2*} on the interior of a single finite element, and of class C^1 across interelement boundaries⁷. A suitable displacement approximation, having extremely good convergence properties, has been introduced by

* A function is taken to be of class C^n if it possesses at least n -continuous, nonzero derivatives within the region of interest.

Bogner, Fox and Schmit⁸. However, that formulation is restricted to rectangular boundaries. In the present analysis, the discretization is performed in natural, or parametric, coordinates, so that any restrictions on the undeformed element geometry can be eliminated. It will be shown that considerable accuracy can be obtained both in displacement and stress prediction by this method of discretization.

Consider first the problem of interpolating a function $F(\xi)$ in one dimension such that continuity of both the function and its slope are everywhere preserved. By requiring the interpolation to reproduce both function and slope exactly at each sampling point one obtains the first order Hermite interpolation formula⁹,

$$F(\xi) = \sum_{j=1}^2 [H_{0j}(\xi)F_j + H_{1j}(\xi)F_{\xi j}], \quad (3.1)$$

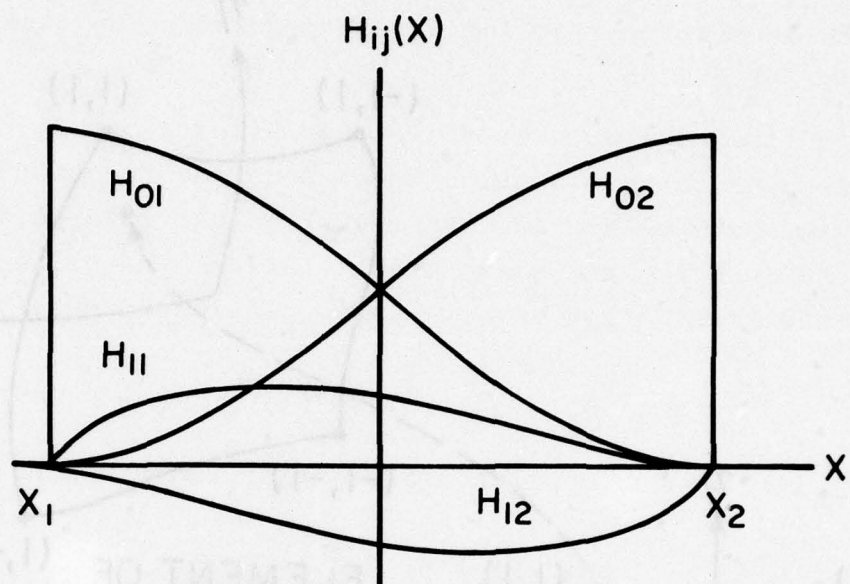
where the $H_{ij}(\xi)$ are cubic polynomials satisfying the conditions

$$\frac{d^n}{d\xi^n} H_{ij}(\xi_k) = \delta_{ni} \delta_{jk}, \quad (3.2)$$

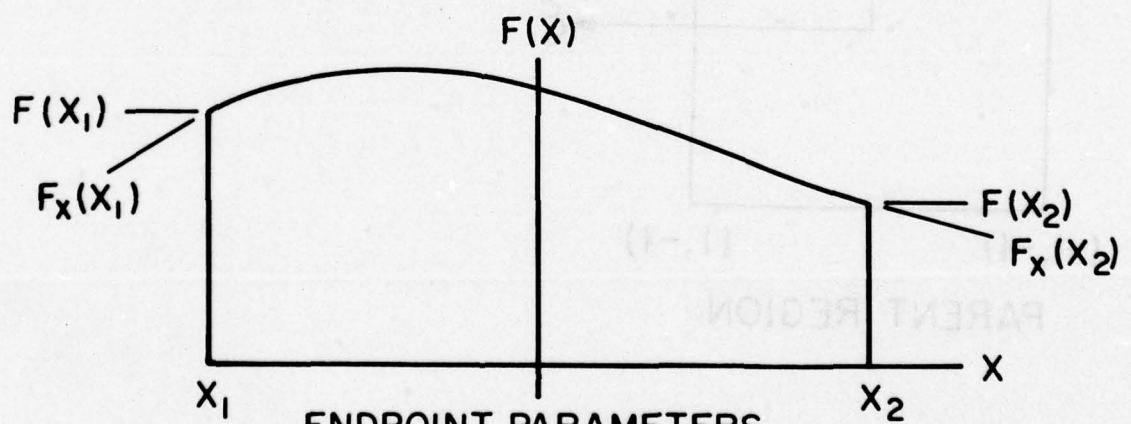
where ξ_k are the interval endpoints (see Figure 3).

For the purpose of obtaining an interpolation formula in a non-rectangular two-dimensional region, a new set of coordinates can be defined within a unit rectangular region which is then related to the true element shape by suitable transformation of coordinates. This new set of "parametric" axes may be thought of as a set of curvilinear coordinates, imbedded within the original geometric region (Figure 4). A function $F(\xi, \eta)$, defined on the rectangular region $-1 \leq (\xi, \eta) \leq 1$, can be represented by the interpolation formula⁸,

$$F(\xi, \eta) = \sum_{i=1}^2 \sum_{j=1}^2 \left[H_{0i}(\xi)H_{0j}(\eta)F_{ij} + H_{1i}(\xi)H_{0j}(\eta)F_{\xi ij} + H_{0i}(\xi)H_{1j}(\eta)F_{\eta ij} + H_{1i}(\xi)H_{1j}(\eta)F_{\xi \eta ij} \right] \quad (3.3)$$



HERMITE POLYNOMIALS



ENDPOINT PARAMETERS

Figure 3. One-Dimensional Hermite Polynomials.

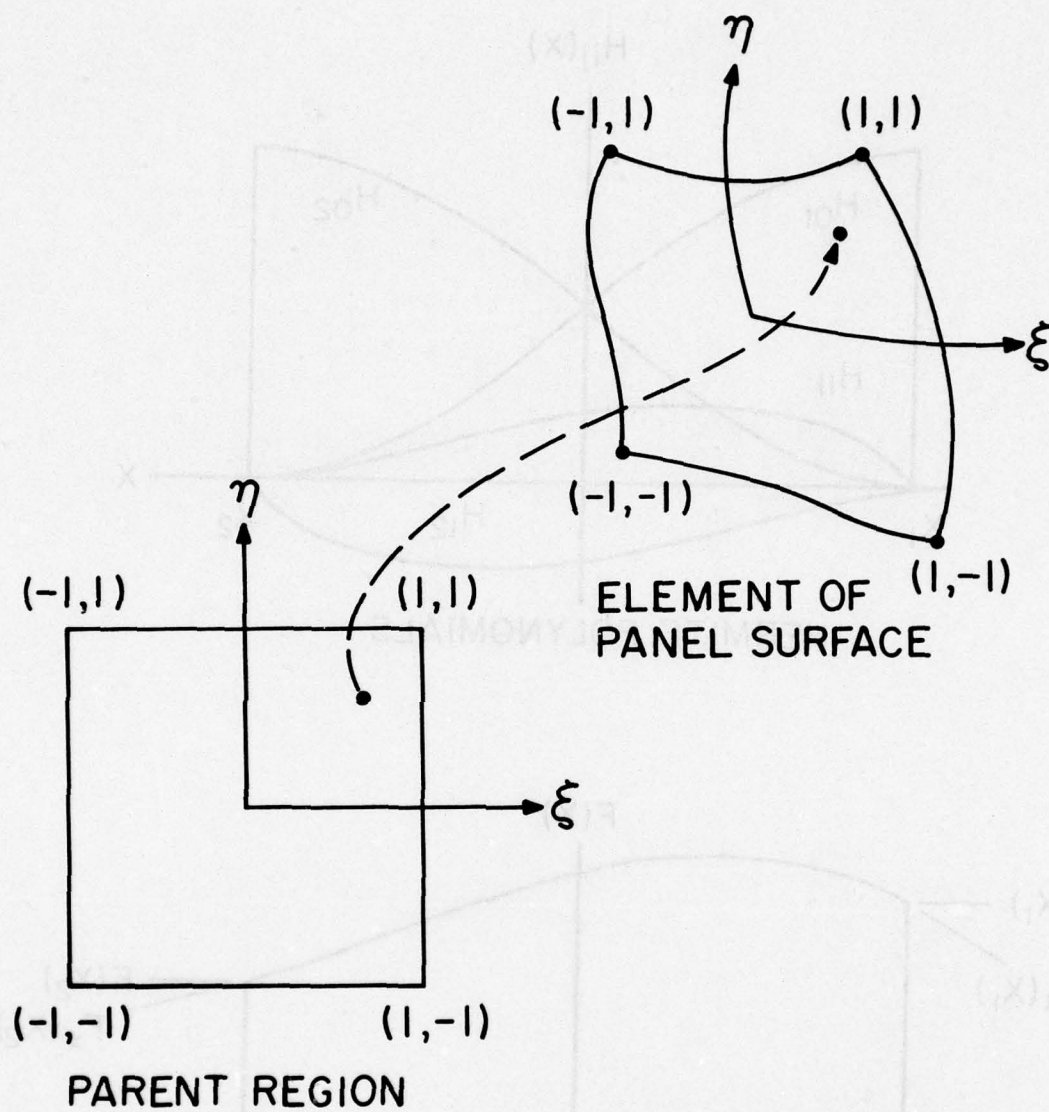


Figure 4. Parametric Coordinate Mapping.

obtained from the product of two one-dimensional formulas having the form of Equation 3.1. On the interval $(\xi_1=-1, \xi_2=+1)$, the Hermite polynomials have the following forms:

$$\begin{aligned} H_{0i}(\xi) &= \frac{1}{4}(1+\xi_i\xi)^2(2-\xi_i\xi) \\ H_{1i}(\xi) &= -\frac{1}{4}\xi_i(1+\xi_i\xi)^2(1-\xi_i\xi); \quad i=1,2. \end{aligned} \quad (3.4)$$

It is important to note that the interpolation takes place within the rectangular region in ξ, η coordinates, and that the nodal parameters $F_{\xi ij}$, $F_{\eta ij}$, $F_{\xi\eta ij}$ represent partial derivatives with respect to the natural coordinates defined within a single element.

The derivatives of each of the displacement components with respect to the natural components (ξ, η) must be related to derivatives in the (x, y) coordinates in order to properly establish the conditions of interelement continuity. By the chain rule, the transformation is of the form

$$\begin{Bmatrix} u_{,\xi} \\ u_{,\eta} \\ \ddot{u}_{,\xi\xi} \\ u_{,\eta\eta} \\ u_{,\xi\eta} \end{Bmatrix} = \begin{bmatrix} x_{,\xi} & y_{,\xi} & 1 & 0 & 0 & 0 \\ x_{,\eta} & y_{,\eta} & 0 & 0 & 0 & 0 \\ x_{,\xi\xi} & y_{,\xi\xi} & x_{,\xi}^2 & -y_{,\xi}^2 & -2x_{,\xi}y_{,\xi} & - \\ x_{,\eta\eta} & y_{,\eta\eta} & x_{,\eta}^2 & y_{,\eta}^2 & 2x_{,\eta}y_{,\eta} & \\ x_{,\xi\eta} & y_{,\xi\eta} & x_{,\xi}x_{,\eta} & y_{,\xi}y_{,\eta} & x_{,\xi}y_{,\eta} + x_{,\eta}y_{,\xi} & \end{bmatrix} \begin{Bmatrix} u_{,x} \\ u_{,y} \\ u_{,xx} \\ u_{,yy} \\ u_{,xy} \end{Bmatrix} \quad (3.5)$$

The above transformation can be obtained from the equations of the region to be considered (for example, the polar coordinate transformation in the case of a circular shape), or by interpolations based upon nodal coordinate data¹⁰. In the present investigation, the transformation indicated in Equation 3.5 is obtained by approximating the spatial coordinate variables in terms of the natural coordinates of an element in the same form as Equation 3.3, and simply differentiating the interpolation formula. Some details and implications of this process are indicated in Paragraph 3.2.

In the present development, all three displacement components in each face of the sandwich panel are represented by the bicubic expansion indicated in Equation 3.3. Although this order of interpolation is greater than the required linear formula for the insurface displacement components, the additional degrees of freedom permit the option of enforcing continuity of membrane strains in adjoining elements. The resulting stress predictions are correspondingly more accurate, and exhibit only minor discontinuities (due to local bending) between elements.

The displacement approximation for a typical finite element is cast into a convenient form as the inner product

$$u_f(\xi, \eta) = \{H(\xi, \eta)\}^T \{U_f\}; \quad f = 1, 2 \quad (3.6)$$

where

$$\{H(\xi, \eta)\}^T = \begin{bmatrix} H_{01}(\xi)H_{01}(\eta), & H_{11}(\xi)H_{01}(\eta), & H_{01}(\xi)H_{11}(\eta), & H_{11}(\xi)H_{11}(\eta), \\ H_{01}(\xi)H_{02}(\eta), & H_{11}(\xi)H_{02}(\eta), & H_{01}(\xi)H_{12}(\eta), & H_{11}(\xi)H_{12}(\eta), \\ H_{02}(\xi)H_{02}(\eta), & H_{12}(\xi)H_{02}(\eta), & H_{02}(\xi)H_{12}(\eta), & H_{12}(\xi)H_{12}(\eta), \\ H_{02}(\xi)H_{01}(\eta), & H_{12}(\xi)H_{01}(\eta), & H_{02}(\xi)H_{11}(\eta), & H_{12}(\xi)H_{11}(\eta) \end{bmatrix} \quad (3.7)$$

and

$$\{U_f\}^T = \begin{bmatrix} u_{f11}, & u_{f\xi11}, & u_{f\eta11}, & u_{f\xi\eta11}, & u_{f12}, & u_{f\xi12}, & u_{f\eta12}, & u_{f\xi\eta12}, \\ 1 \times 16 & u_{f22}, & u_{f\xi22}, & u_{f\eta22}, & u_{f\xi\eta22}, & u_{f21}, & u_{f\xi21}, & u_{f\eta21}, & u_{f\xi\eta21} \end{bmatrix}. \quad (3.8)$$

The remaining displacement functions $v_f(\xi, \eta)$ and $w_f(\xi, \eta)$ have similar forms. A displacement vector for the entire sandwich element is then assembled in the form

$$\{U_E\}^T = \begin{bmatrix} \{U_1\}^T, & \{U_2\}^T, & \{v_1\}^T, & \{v_2\}^T, & \{w_1\}^T, & \{w_2\}^T \end{bmatrix}. \quad (3.9)$$

1x96

The resulting sandwich element therefore possesses 96 external degrees of freedom.

It should be noted that since the unknown displacements within the entire sandwich panel are expressed in terms of the face sheet

displacements, the consideration of multicore constructions presents no particular problem. Two or more sandwich elements can be "stacked" to represent multicore geometry, simply by the proper specification of element connectivity data. The displacement vectors (Equation 3.9) of stacked elements are joined in exactly the same manner as for two adjacent planar elements during the accumulation of the system equations.

3.2 Parametric Mapping Considerations

In most applications of the isoparametric element formulation (e.g., solids, plane-stress elements), only the physical displacements are needed as nodal parameters. However, the requirement of slope continuity in elements based upon the Kirchhoff assumption necessitates the use of derivatives of the displacements as nodal variables to fulfill the conditions of interelement compatibility. Since the displacement derivatives are computed in parametric coordinates, it is instructive to consider the constraints placed upon the geometric mapping by displacement compatibility conditions on the interelement boundaries.

For the enforcement of displacement (but not slope) continuity on an interelement boundary, examination of Equation 3.3 reveals that the displacement at any point on the boundary depends upon the nodal displacement values and parametric derivatives tangent to the boundary, evaluated at the endpoints of the edge. Thus, it is sufficient to require that the parametric coordinate tangent to the interelement boundary be the same for any two adjacent elements on their common edge. Such a requirement presents no difficulty, even for mappings of a very general nature.

The need for slope continuity between adjoining finite elements is a somewhat more subtle problem. Consider first the establishment of slope continuity between adjacent rectangular elements (Figure 5). It is easily shown using Equation 3.2 that a matching of the parametric derivatives and cross-derivatives at common vertices produces continuity of transverse slopes in parametric space along the entire boundary¹¹. Thus, if the mapping $x=x(\xi, \eta)$ and $y=y(\xi, \eta)$

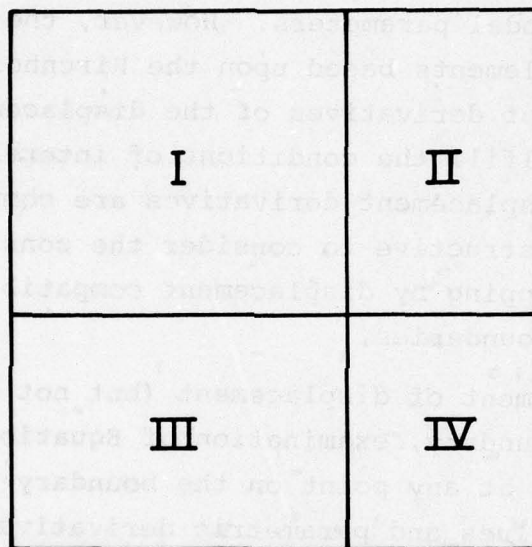


Figure 5. Adjacent Rectangular Elements.

possesses continuous first derivatives on the common boundaries, the physical slopes ($w_{,x}$ and $w_{,y}$) are made continuous as well whenever $w_{\xi ij}$, $w_{\eta ij}$ and $w_{\xi\eta ij}$ are matched at the boundary endpoints. For non-rectangular elements (Figure 6), compatibility of the physical slopes is obtained under similar conditions. However, since the transformation from parametric to physical coordinates may now have nonzero second derivatives, one must examine the conditions under which equality of the cross-derivatives $w_{\xi\eta ij}$ at the common nodes is admissible. For two adjoining elements of identical thickness, Equation 3.5 dictates that a matching of $w_{\xi\eta ij}$ at common vertices is permitted only if the transformation of coordinates possesses continuous first derivatives on the interelement boundaries and continuous second derivatives at the nodal points.

Under the conditions stated above, equality of w_{ij} , $w_{\xi ij}$, $w_{\eta ij}$ and $w_{\xi\eta ij}$ ensures the continuity of w , $w_{,\xi}$ and $w_{,\eta}$ (and hence that of $w_{,x}$ and $w_{,y}$) along the common edges of adjacent elements. For most problems having reasonable geometries, no particular problems are encountered in establishing an acceptable mapping; in the most general case, conditions of compatibility can be satisfied by the enforcement of linear constraints between nodal variables involving parametric derivatives.

In the present development, the geometric mapping between the physical and parametric forms of a single finite element is based upon the same interpolation formula as the displacement approximation:

$$\begin{aligned} x(\xi, \eta) &= \{H(\xi, \eta)\}^T \{X\} \\ y(\xi, \eta) &= \{H(\xi, \eta)\}^T \{Y\} \end{aligned} \quad (3.10)$$

The vectors $\{X\}$ and $\{Y\}$ contain values of x, y and their derivatives with respect to the parametric coordinates ξ, η evaluated at the nodes of an element. The geometric mapping given by Equation 3.10 is identical to the well-known "surface patch" representation introduced by Coons¹². Palacol and Stanton¹⁰ have adapted the bicubic patch method to the analysis of thin orthotropic plates and achieved excellent results.

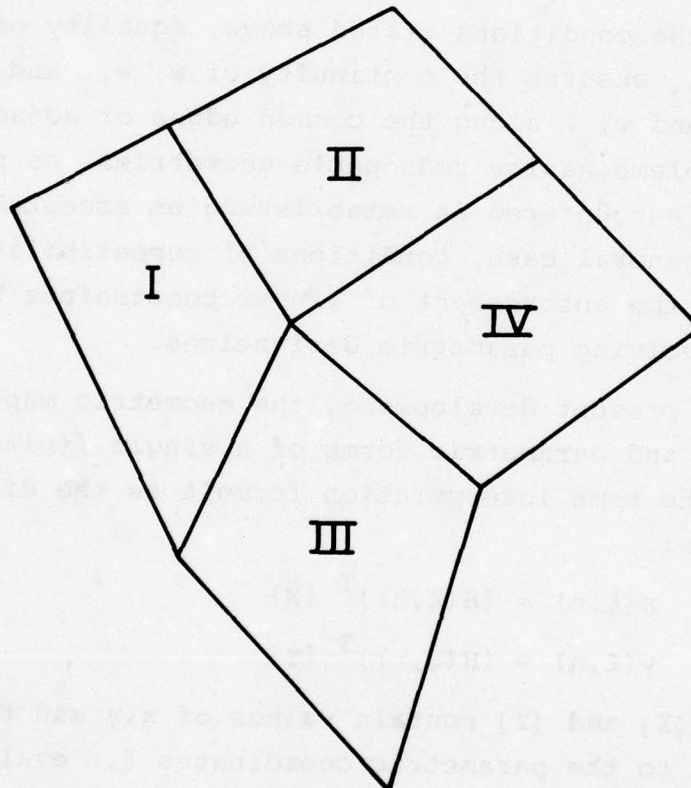


Figure 6. Adjacent Nonrectangular Elements.

By means of Equation 3.10, the problem of representing irregular geometries in the undeformed state is reduced to the selection of an acceptable set of mapping parameters $\{X\}$ and $\{Y\}$ at the nodal points. For many shapes, the parameters may be obtained analytically. As an example consider the circular element sector shown in Figure 7. Taking $r(\eta)$ and $\theta(\xi)$ to be linear functions,

$$\begin{aligned} r &= r_0 + \frac{1}{2} (1+\eta) \Delta r \\ \theta &= \frac{1}{2} (1-\xi) \Delta \theta \end{aligned} \quad (3.11)$$

the polar coordinate transformation yields $x(\xi, \eta)$, $y(\xi, \eta)$ explicitly as

$$\begin{aligned} x &= [r_0 + \frac{1}{2}(1+\eta)\Delta r] \cos \frac{1}{2}(1-\xi)\Delta \theta \\ y &= [r_0 + \frac{1}{2}(1+\eta)\Delta r] \sin \frac{1}{2}(1-\xi)\Delta \theta \end{aligned} \quad (3.12)$$

The vector $\{X\}$, for example, contains the entries

$$\{X\}^T = [x_1, x_{\xi 1}, x_{\eta 1}, x_{\xi \eta 1}, x_2, \dots, x_{\xi \eta 4}] \quad (3.13)$$

For the annular sector, from Equation 3.12,

$$\begin{aligned} \{X\}^T = & \begin{bmatrix} r_0 \cos \Delta \theta & , & \frac{1}{2} r_0 \Delta \theta \sin \Delta \theta & , \\ \frac{1}{2} \Delta r \cos \Delta \theta & , & \frac{1}{4} \Delta r \Delta \theta \sin \Delta \theta & , \\ (r_0 + r) \cos \Delta \theta & , & \frac{1}{2} (r_0 + \Delta r) \Delta \theta \sin \Delta \theta & , \\ \frac{1}{2} \Delta r \cos \Delta \theta & , & \frac{1}{4} \Delta r \Delta \theta \sin \Delta \theta & , \\ r_0 + \Delta r & , & 0 & , \\ \frac{1}{2} \Delta r & , & 0 & , \\ r_0 & , & 0 & , \\ \frac{1}{2} \Delta r & , & 0 & , \end{bmatrix}. \end{aligned} \quad (3.14)$$

As a second example, consider the elliptical element shown in Figure 8. By taking the element edges along concentric elliptical lines and lines of constant angle θ , the following description of the boundary curves of an element is obtained:

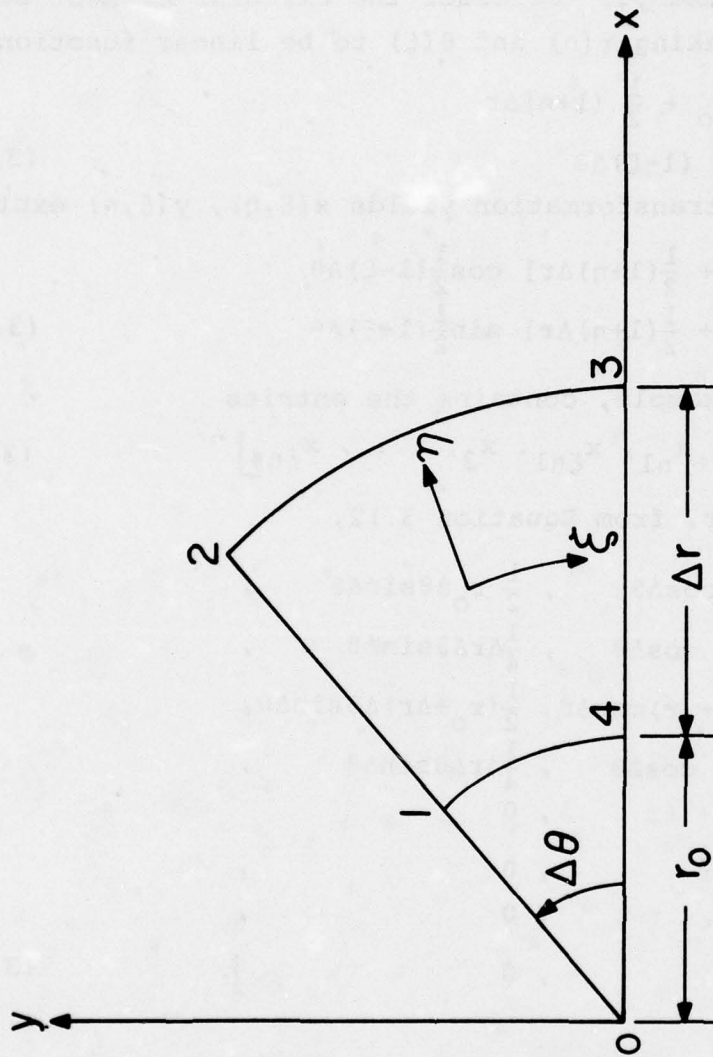


Figure 7. Circular Element Sector.

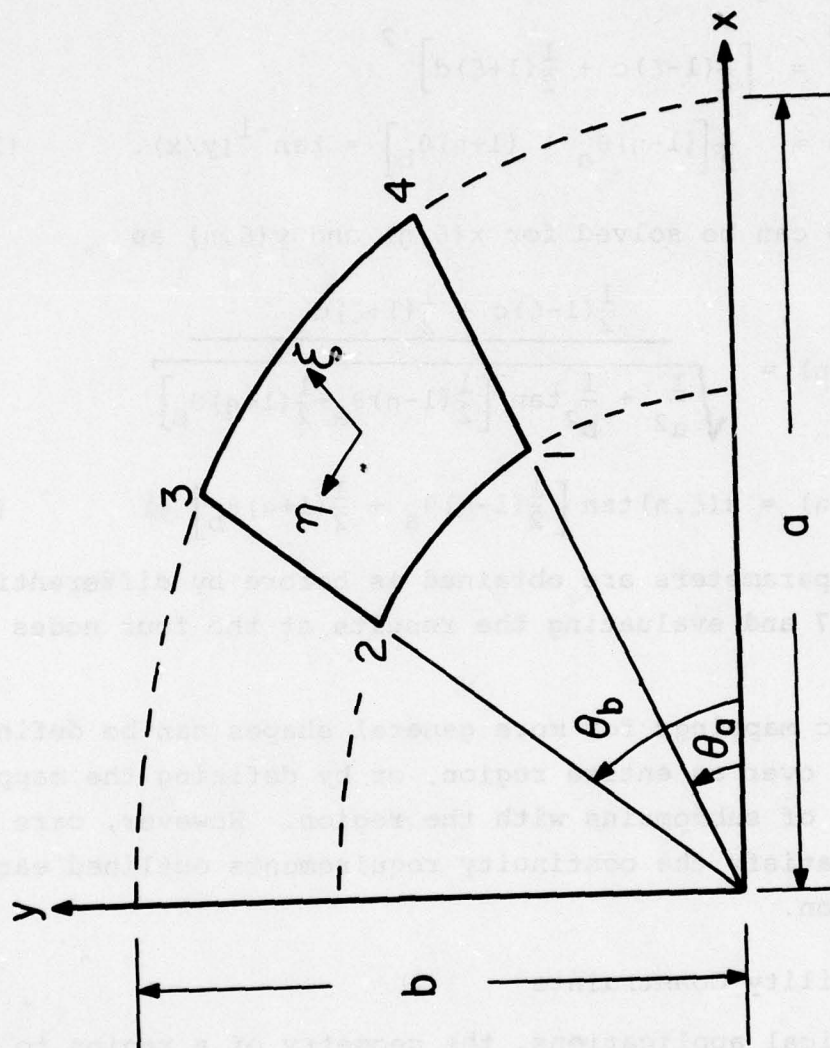


Figure 8. Elliptical Element Sector.

$$\begin{aligned}
\text{Line 1-2: } & (x/a)^2 + (y/b)^2 = c^2 \\
\text{Line 3-4: } & (x/a)^2 + (y/b)^2 = d^2 \\
\text{Line 1-4: } & \theta = \theta_a \\
\text{Line 2-3: } & \theta = \theta_b
\end{aligned} \tag{3.15}$$

Let

$$\begin{aligned}
\left(\frac{x}{2}\right)^2 + \left(\frac{y}{b}\right)^2 &= \left[\frac{1}{2}(1-\xi)c + \frac{1}{2}(1+\xi)d\right]^2 \\
\theta &= \frac{1}{2}[(1-\eta)\theta_a + (1+\eta)\theta_b] = \tan^{-1}(y/x).
\end{aligned} \tag{3.16}$$

Equations 3.16 can be solved for $x(\xi, \eta)$ and $y(\xi, \eta)$ as

$$\begin{aligned}
x(\xi, \eta) &= \frac{\frac{1}{2}(1-\xi)c + \frac{1}{2}(1+\xi)d}{\sqrt{\frac{1}{a^2} + \frac{1}{b^2} \tan^2\left[\frac{1}{2}(1-\eta)\theta_a + \frac{1}{2}(1+\eta)\theta_b\right]}} \\
y(\xi, \eta) &= x(\xi, \eta) \tan\left[\frac{1}{2}(1-\eta)\theta_a + \frac{1}{2}(1+\eta)\theta_b\right]
\end{aligned} \tag{3.17}$$

The patching parameters are obtained as before by differentiating Equations 3.17 and evaluating the results at the four nodes of the element.

Geometric mappings for more general shapes can be defined by interpolating over an entire region, or by defining the mappings over a number of subdomains with the region. However, care must be taken to satisfy the continuity requirements outlined earlier in this section.

3.3 Compatibility Constraints

In practical applications, the geometry of a region to be modelled often requires that the parametric coordinate mappings in adjacent elements possess discontinuous derivatives. An example is shown in Figure 9. For the case shown, the natural coordinate η is the same in both elements, but the relationships $x=x(\xi, \eta)$, $y=y(\xi, \eta)$ exhibit discontinuous ξ -derivatives on the common boundary. Although the continuity of w (which depends

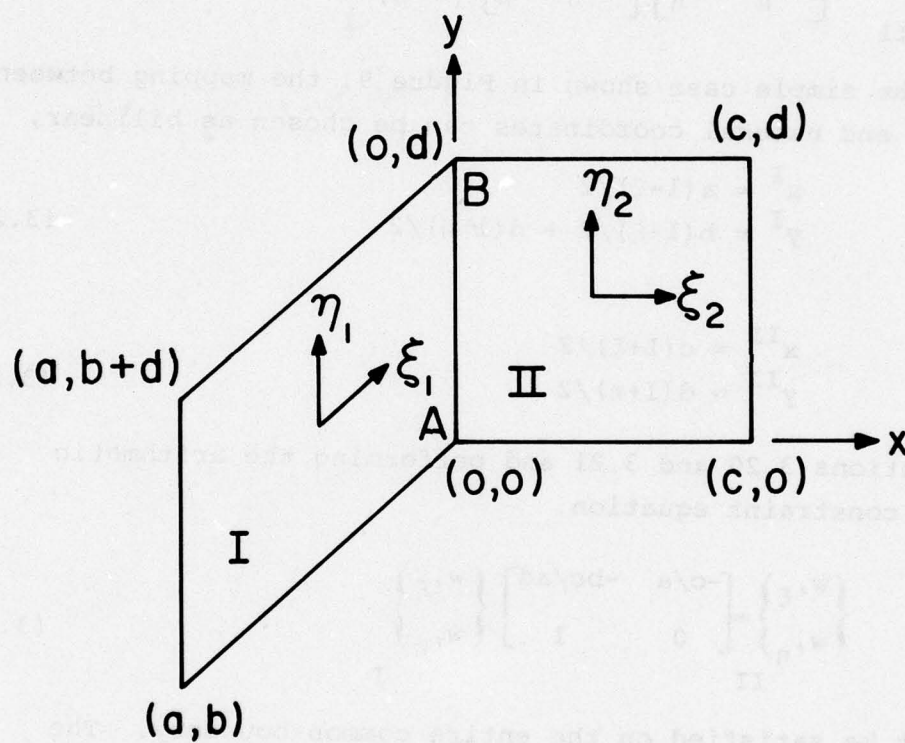


Figure 9. Adjacent Elements Requiring Compatibility Constraints.

only on the nodal values w_{ij} and w_{nij}) on the common edge presents no particular problem, it is required that the slopes in physical coordinates, $w_{,x}$ and $w_{,y}$, be everywhere continuous on the boundary. The required conditions of continuity are found by setting

$$\begin{Bmatrix} w_{,x} \\ w_{,y} \end{Bmatrix}_I = \begin{Bmatrix} w_{,x} \\ w_{,y} \end{Bmatrix}_{II} \quad (3.18)$$

or

$$\begin{Bmatrix} w_{,\xi} \\ w_{,\eta} \end{Bmatrix}_{II} = \begin{bmatrix} x_{,\xi}^{II} & y_{,\xi}^{II} \\ x_{,\eta} & y_{,\eta} \end{bmatrix} \begin{bmatrix} x_{,\xi}^I & y_{,\xi}^I \\ x_{,\eta} & y_{,\eta} \end{bmatrix}^{-1} \begin{Bmatrix} w_{,\xi} \\ w_{,\eta} \end{Bmatrix}_I \quad (3.19)$$

For the simple case shown in Figure 9, the mapping between the global and natural coordinates can be chosen as bilinear,

$$\begin{aligned} x^I &= a(1-\xi)/2 \\ y^I &= b(1-\xi)/2 + d(1+\eta)/2 \end{aligned} \quad (3.20)$$

and

$$\begin{aligned} x^{II} &= c(1+\xi)/2 \\ y^{II} &= d(1+\eta)/2 \end{aligned} \quad (3.21)$$

Using Equations 3.20 and 3.21 and performing the arithmetic gives the constraint equation

$$\begin{Bmatrix} w_{,\xi} \\ w_{,\eta} \end{Bmatrix}_{II} = \begin{bmatrix} -c/a & -bc/ad \\ 0 & 1 \end{bmatrix} \begin{Bmatrix} w_{,\xi} \\ w_{,\eta} \end{Bmatrix}_I \quad (3.22)$$

which must be satisfied on the entire common boundary. The second equation, which reflects the fact that η is identical in both elements on their common edge, need not be considered further. The remaining equation,

$$w_{,\xi}^{II} = -\frac{c}{a}(w_{,\xi}^I + \frac{b}{d}w_{,\eta}^I) \quad (3.23)$$

must be expressed in terms of the nodal parameters at the points A,B to arrive at the final constraint relations. Using the element interpolation functions (Equation 3.6), Equation 3.23 can be expressed as a polynomial in η , whose coefficients are the nodal variables at A and B in elements I and II. By requiring the coefficient of each power of η to vanish, one arrives at the discrete form of the constraint relations,

$$\begin{Bmatrix} w_{\xi A} \\ w_{\xi B} \\ w_{\xi \eta A} \\ w_{\xi \eta B} \end{Bmatrix}_I = \frac{c}{2a} \begin{bmatrix} 0 & 0 & -2 & 0 & -2\frac{b}{d} & 0 & 0 & 0 \\ 0 & 0 & 1 & -3 & 0 & -2\frac{b}{d} & 1 & 1 \\ 3\frac{b}{d} & -3\frac{b}{d} & 0 & 0 & 4\frac{b}{d} & 2\frac{b}{d} & -2 & 0 \\ -3\frac{b}{d} & 3\frac{b}{d} & 0 & 0 & -2\frac{b}{d} & -4\frac{b}{d} & 0 & -2 \end{bmatrix} \begin{Bmatrix} w_A \\ w_B \\ w_{\xi A} \\ w_{\xi B} \\ w_{\eta A} \\ w_{\eta B} \\ w_{\xi \eta A} \\ w_{\xi \eta B} \end{Bmatrix}_{II} \quad (3.24)$$

Similar constraints to ensure interelement compatibility of displacement and transverse slopes can be evaluated for more general element shapes and orientations. Equation 3.19 is again used as a starting point, but the required constraints can become considerably more complicated than Equation 3.24. In such cases the calculations are best performed numerically, in terms of the mapping parameters of an element.

It should be noted that in most cases, an acceptable parametric mapping can be constructed even in the presence of highly irregular geometries. For example, the above case can be considered without the imposition of linear constraints, even though the physical boundary slopes approaching the edge at $x = 0$ are double-valued. Instead of the bilinear form, consider the mappings

$$\begin{aligned} x(\xi, \eta) &= \frac{a}{8} (1 - 3\xi + 3\xi^2 - \xi^3) \\ y(\xi, \eta) &= \frac{b}{8} [1 - 3\xi + 3\xi^2 - \xi^3 + 4\frac{d}{b} (1 - \eta)] \end{aligned} \quad (3.25)$$

and

$$\begin{aligned} x(\xi, \eta) &= \frac{c}{8} (1 + 3\xi + 3\xi^2 + \xi^3) \\ y(\xi, \eta) &= \frac{d}{2} (1 + \eta) \end{aligned} \quad (3.26)$$

for elements I and II respectively. It is easily verified that the above parametric mappings are twice continuously differentiable across the common boundary, which is more than adequate to ensure interelement displacement and slope compatibility.

SECTION 4

NUMERICAL CONSIDERATIONS

The selection of the best and most efficient numerical analysis is an important consideration in the implementation of any finite element procedure. In particular, the calculation of refined element representations and the evaluation of nonlinear effects must be done efficiently if the analysis program is to be cost effective.

In this section, a number of aspects of the process of setting up and solving the finite element equations are discussed. Many of the details involved in implementation of the finite element technique are widely accepted¹³, and will not be repeated here. The computational techniques considered are those less common in finite element analysis, or developed specifically for use with the present method.

4.1 Calculation of Element Stiffness Matrices

The computation of the linear stiffness matrix (corresponding to quadratic terms in the potential energy, Equation 2.26) is considered below. Evaluation of the nonlinear potential energy and the energy gradient for large-displacement problems is discussed in the following section.

Since the element geometry is not predetermined, it is necessary to perform numerical integrations to obtain the element stiffness. The most common method gives for the stiffness matrix the integral¹⁴

$$[K]_e = \int_{-1}^1 \int_{-1}^1 [N]^T [B]^T [D] [B] [N] |J| d\xi d\eta \quad (4.1)$$

where $[N]$ is a matrix of polynomial functions, $[B]$ is the strain-displacement relationship and $[D]$ is a matrix of elastic constants. The integration can be carried out by Gaussian quadrature, with the integrand being evaluated at each of a number of sampling points.

The above method of integration is not practical in the present case, since the order of the matrices is large (the element matrix, $[K]_e$, is of order 96), and because many integration points are required for the exact evaluation of the higher-order polynomial functions. By taking advantage of repetitive patterns occurring in the polynomial terms in the original functional (Equation 2.26), the number of operations required for the evaluation of Equation 4.1 can be reduced by a factor of approximately 250, thereby reducing substantially the amount of computing time required for setting up the system of equations to be solved.

In the potential energy (Equation 2.26), each quadratic term can be expressed in the form

$$T = \iint c u_{f,ij}^{\alpha} u_{f,kl}^{\beta} dx dy, \quad (4.2)$$

where c represents a material constant, u_f^{α} and u_f^{β} denote the components of displacement u_f , v_f , or w_f within a single face sheet, and the indices i, j, k, l indicate the appropriate spatial derivatives of the displacement components. Restricting the discussion to cases for which c is constant over the element, the use of Equation 3.6 gives

$$\begin{aligned} T = & \frac{c}{2} \{u_f^{\alpha}\}^T \iint \{H_{,ij}\} \{H_{,kl}\}^T dx dy \{u_f^{\beta}\} \\ & + \frac{c}{2} \{u_f^{\beta}\}^T \iint \{H_{,kl}\} \{H_{,ij}\}^T dx dy \{u_f^{\alpha}\} \end{aligned} \quad (4.3)$$

Thus, regardless of the values of α, β , only the 16×16 matrix

$$\iint \{H_{,ij}\} \{H_{,kl}\}^T dx dy \quad (4.4)$$

and its transpose must be evaluated for each combination of i, j, k and l in order to calculate all of the possible combinations to the stiffness matrix. The number of combinations of i, j, k and l is further reduced when only the upper triangle of the element matrix is considered, since the component matrices can be transposed when required during the actual assembly of the matrix.

The numerical integration indicated in Equation 4.4 is performed as follows. At a particular integration point, the vector $\{H(\xi, \eta)\}$ (Equation 3.7) and its derivatives with respect to the coordinates (ξ, η) are computed, and transformed by the chain rule to $(x-y)$ -derivatives. The resulting vectors are multiplied by the square root of the product of the Gaussian weight and the Jacobian determinant, to reduce later computations. Finally, all possible outer products of the vectors $\{H_{ij}\}$ and $\{H_{kl}\}$ are formed, and the sums accumulated over an $n \times n$ grid of integration points.* Having formed the component matrices, it remains only to multiply through by the appropriate elastic constants and accumulate the products into the element stiffness matrix.

It is significant that numerical experiments performed using Equation 4.1 with a 4×4 integration grid and eliminating the multiplication of all-zero submatrices, yield computing times on the CDC-6600 of more than 120 seconds for a single element stiffness matrix. The above method using component matrices requires approximately one-half second on the same machine, using the default level of compiler optimization. This amount of computation is approximately the same as that expended in the stiffness calculation for the well-known 20-node (60 d.o.f.) solid element using a $3 \times 3 \times 3$ integration grid. The half-second computation time for a single element matrix can be made even less by further compiler optimization of the code.

4.2 Evaluation of the Nonlinear Strain Energy

In the present analysis, the solution to the nonlinear problem is obtained by seeking a minimum of the potential energy functional directly. Hence, only the potential energy and its gradient with respect to the unknown displacement parameters must be evaluated

* Polynomial terms of degree $2n-1$ are therefore integrated exactly. Integration with $n=4$ is sufficient for most geometries.

(see Section 4.3). Since the function and gradient evaluation represents a large portion of the total solution time, and must be performed a number of times, it is important to organize the computations as efficiently as possible. The numerical integrations upon which the calculation of the linearized stiffness matrix is based (Section 4.1) provide a means of obtaining all of the information required for evaluation of the nonlinear strain energy terms, so that very little added computation is necessary.

Consider first the linearized potential energy, which can be expressed as

$$\pi_p^{(\ell)} = \frac{1}{2} \{U\}^T [K] \{U\} - \{U\}^T \{P\} \quad (4.5)$$

since the global stiffness matrix $[K]$ is symmetric, the required gradient is given by

$$\nabla \pi_p^{(\ell)} = [K] \{U\} - \{P\}. \quad (4.6)$$

The direct evaluation of Equations 4.5 and 4.6 is the most efficient means of carrying out the computation, when the common terms and matrix symmetry are taken into account. Although it is not necessary to form a global stiffness matrix (indeed, this feature has often been cited as an advantage of minimization methods of solution), the evaluation of the potential energy and its gradient element-by-element is a relatively inefficient process. A count of the multiplications* and input-output operations required is evidence of this fact.

As an example of the evaluation of the nonlinear terms of the strain energy, consider the cubic term

$$\tau = \int \int_{A_f} C u_{f,ij}^{\alpha} u_{f,k\ell}^{\beta} u_{f,mn}^{\gamma} dx dy \quad (4.7)$$

* On the CDC 6000 series computers, where memory-access operations can consume somewhat more time than floating-point arithmetic, a similar argument holds in favor of the present method.

where the notation is that used in the previous section. For the purpose of evaluating the term itself, it is convenient to evaluate $u_{f,ij}^\alpha$, $u_{f,kl}^\beta$ and $u_{f,mn}^\gamma$ directly, using the vectors $\{H_{ij}\}$ of Equation 4.4 and the element displacement vector $\{U_E\}$ (Equation 3.9). This computation is made at each Gaussian quadrature point, and the weighted sums accumulated to evaluate T . The computational expense involved is small, since the vectors $\{H_{ij}\}$ have already been calculated at each integration point during the linear stiffness matrix evaluation. Furthermore, only a limited number of terms of the form $u_{f,ij}^\alpha$ appear in the energy, and repetitive patterns are easily taken into account.

Evaluation of the gradient of Equation 4.7 is performed in a similar manner. Since

$$u_{f,ij}^\alpha = \{H_{ij}\}^T \{U_f^\alpha\}, \quad (4.8)$$

the cubic term can be rewritten in the form

$$\begin{aligned} T = & C \iint_{A_f} \{H_{ij}\}^T u_{f,kl}^\beta u_{f,mn}^\gamma dx dy \{U_f^\alpha\} \\ & + C \iint_{A_f} u_{f,ij}^\alpha \{H_{kl}\}^T u_{f,mn}^\gamma dx dy \{U_f^\beta\} \\ & + C \iint_{A_f} u_{f,ij}^\alpha u_{f,kl}^\beta \{H_{mn}\}^T dx dy \{U_f^\gamma\} \end{aligned} \quad (4.9)$$

When α is different from β and γ , the gradient of T with respect to the entries of $\{U_f^\alpha\}$ is given by

$$\frac{\partial T}{\partial \{U_f^\alpha\}_p} = C \iint_{A_f} \{H_{ij}\}_p^T u_{f,kl}^\beta u_{f,mn}^\gamma dx dy \quad (4.10)$$

and again the integration is carried out numerically. Since each of the individual terms in Equation 4.10 has been at least partially evaluated in evaluating the energy function, the total gradient evaluation requires only a small amount of additional computation.

Alternative methods of organizing the calculation of nonlinear strain energy contributions have commonly employed very large matrices, whose entries are associated with each of the possible combinations of nodal variables within individual elements^{3,15}. Such techniques often require excessive amounts of storage (for the present element, a vector of length 9316 would have to be saved for each element merely for the evaluation of quartic terms in the strain energy) and input-output time. The present method uses a minimal amount of core storage, since only a single vector of length $80n^2$ is needed for each element, where n^2 is the number of Gaussian integration points. It is clear that the computational procedure described here represents a very effective approach for use in the solution of problems involving geometric nonlinearities.

4.3 Solution of the System of Nonlinear Equations

In the present analysis, a solution is sought by direct minimization of the discrete potential energy with respect to the undetermined nodal displacement parameters. The solution process is therefore one of unconstrained function minimization. Gradient methods of minimization have been shown to be the most powerful class of solution techniques for such problems¹⁶. Two such methods which have been implemented in the present analysis are described in the following section.

4.3.1 Fletcher-Powell Algorithm

The Fletcher-Powell (or variable metric) method of minimization bears a close resemblance to the familiar Newton-Raphson iteration. However, the Fletcher-Powell technique makes use of an approximate metric in place of the matrix of exact second derivatives during each iteration. The algorithm, originally suggested by Davidon¹⁷ and improved upon by Fletcher and Powell¹⁸, is quadratically convergent and possesses extremely good stability properties.

Given a function $F(\vec{X})$ which is to be minimized, the Fletcher-Powell iteration proceeds as follows:

1. An initial estimate of \vec{X}_0 of the solution is selected. Usually this estimate consists of a linear solution, or an extrapolation of previous nonlinear solutions.

2. The gradient of F is computed, and an initial search direction \vec{S}_0 is selected along the direction of steepest descent; that is,

$$\vec{S}_0 = -[H]_0 \nabla F(\vec{X}_0) \quad (4.11)$$

where $[H]_0$ is the identity matrix.

3. A value of α is determined in such a way that $F(\vec{X}_i + \alpha \vec{S}_i)$ is minimized.

4. The vector of unknowns is updated by

$$\vec{X}_{i+1} = \vec{X}_i + \alpha \vec{S}_i \quad (4.12)$$

5. The following quantities are calculated:

$$\vec{Y}_i = \nabla F(\vec{X}_{i+1}) - \nabla F(\vec{X}_i) \quad (4.13)$$

$$[M]_i = \alpha_i \frac{\vec{S}_i \vec{S}_i^T}{\vec{S}_i^T \vec{Y}_i} \quad (4.14)$$

$$[N]_i = - \frac{([H]_i \vec{Y}_i) ([H]_i \vec{Y}_i)^T}{\vec{Y}_i^T [H]_i \vec{Y}_i} \quad (4.15)$$

6. A new metric is computed from

$$[H]_{i+1} = [H]_i + [M]_i + [N]_i \quad (4.16)$$

7. A new search direction is determined according to

$$\vec{S}_{i+1} = -[H]_{i+1} \nabla F(\vec{X}_{i+1}) \quad (4.17)$$

and steps 3 through 7 are repeated until convergence is achieved.

The Fletcher-Powell technique exhibits extremely fast convergence in practice, and is particularly effective when a scaling transformation is used to normalize the vector \vec{X} of unknowns¹⁶. The scaling implemented in the present analysis adjusts the unknown variables according to the diagonal elements of the linearized stiffness matrix, since these constitute a rough approximation to the second derivatives of the function.

The primary disadvantage of the Fletcher-Powell minimization is the need to retain a full matrix $[H]_i$ at each step, since storage requirements may become excessive for larger problems. This limitation is eliminated altogether with the Fletcher-Reeves algorithm, as discussed in the following section. For smaller problems, however, the Fletcher-Powell scheme is possibly the most powerful of the gradient methods of minimization, and is preferred over the Fletcher-Reeves procedure.

4.3.2 Fletcher-Reeves Algorithm

The Fletcher-Reeves (or conjugate gradient) method of minimization¹⁹ is similar to the variable metric technique, but utilizes a less involved method of selecting a direction for search. In this case, the information retained about higher derivatives of the function consists of a single vector, rather than a full matrix. The current search direction \vec{S} is then selected according to

$$\beta_i = \frac{|\nabla F(\vec{X}_i)|^2}{|\nabla F(\vec{X}_{i-1})|^2} \quad (4.18)$$

and

$$\vec{S}_i = -\nabla F(\vec{X}_i) + \beta_i \vec{S}_{i-1} \quad (4.19)$$

replacing steps 5 through 7 of the Fletcher-Powell algorithm (Equations 4.13 through 4.17).

It can be seen that the computer storage requirements for the conjugate-gradient algorithm are substantially

less than for the Fletcher-Powell procedure. However, even though the Fletcher-Reeves method is theoretically quadratically convergent, convergence difficulties can arise in practice due to successive roundoff accumulated in the \vec{S} vector from iteration to iteration. Periodic restarts of the iteration are therefore often necessary, and convergence may require substantially more effort than is theoretically expected. A thorough discussion of this problem, with numerical examples, is presented in Reference 20.

Substantial improvement in the performance of the Fletcher-Reeves minimization is obtained by virtue of the scaling transformation mentioned in the previous section. This modification of the problem serves to minimize the eccentricity of the function space under consideration, thus improving the numerical behavior of the iterations. A number of examples demonstrating the effects of the scaling transformation are cited in Reference 16.

SECTION 5

COMPUTER PROGRAM

The sandwich finite element analysis reported herein has been implemented in a computer program, which is briefly described in this section. Both linear and nonlinear analyses can be performed with the program, and multiple-pass capability is provided for nonlinear problems. Although the code has been developed on the CDC 6600 computer, it can be made compatible with other machines with relatively few modifications.

5.1 Program Size and Capacity

The sandwich finite element code presently consists of slightly more than 5000 FORTRAN statements, distributed among 68 subroutines and the main program. Although the compiled program occupies less than 70,000 (octal) storage locations on the CDC 6600, linear problems having up to 6000 degrees of freedom and nonlinear problems of more than 1000 degrees of freedom can be accommodated. These limits are easily adjusted upward by modifying appropriate array-dimensioning statements. Multiple load cases may be considered for linear analysis. Three types of finite elements (plates, cylindrical shells, flat sandwich panels) are presently available in the program; all of these are based upon the bicubic interpolation scheme outlined in Section 3.1.

5.2 Program Organization

The computer program is arranged in modular form, and utilizes the CDC segmentation loader²¹ to obtain a maximum of flexibility in ordering the computations. The segmented structure allows for a greater subdivision of the computational tasks than is feasible with the conventional overlay organization, and hence larger problems may be considered with quite modest central memory requirements. Furthermore, provision for creating "copies"

of certain commonly-used service routines makes these routines available to the necessary sections of the program, even though they are not retained in high-speed memory during the entire problem solution.

All internal data is normally kept on disk files, in contrast to an "overflow" type of data structure. The motivation for this is the large number of degrees of freedom involved in a single element (96 for the flat sandwich panel element), so that problems considered by the program would normally be solved out-of-core regardless of the data organization. The handicap for small problems is minimal, as shown in Section 5.3.

Five different equation-solving routines are presently available to the finite element analysis. For linear problems, an in-core band solution or an out-of-core block solver are provided; a conjugate gradient (Section 4.3.2) algorithm and two versions of the variable metric (Section 4.3.1) solution (in-core and out-of-core) are implemented for nonlinear analysis. The method of equation solution is chosen according to problem type, problem size, and available memory, as indicated in Table 1.

The present computer code contains partial generation capabilities for nodal coordinates, element connectivity and boundary condition data, to reduce the effort required by the user. Geometry data and distributed loadings may alternatively be described in equation form through the use of user-written subroutines. A partial restart capability is also provided for use in nonlinear analysis.

5.3 Computing Time and Memory Requirements

Memory allocation for the present finite element analysis program is diagrammed in Figure 10, according to blocks of routines which represent major steps in the computational procedure. The maximum field length requirement is 67740 octal words of memory, with this being determined by the storage required for the nonlinear solution. Linear solutions can be

TABLE 1
AVAILABLE EQUATION SOLUTION METHODS

Method of Solution	Problem Type	Problem Size	Amount of High Speed Storage Required
In-core Band Solution	Linear	Small	(variable)
Out-of-core Block Solution	Linear	Medium-Large	Small-Medium
Conjugate Gradient	Linear/Nonlinear	Medium-Large	Small-Medium
Variable Metric I (in-core)	Linear/Nonlinear	Small-Medium	Medium
Variable Metric II (out-of-core)	Linear/Nonlinear	Medium-Large	Medium

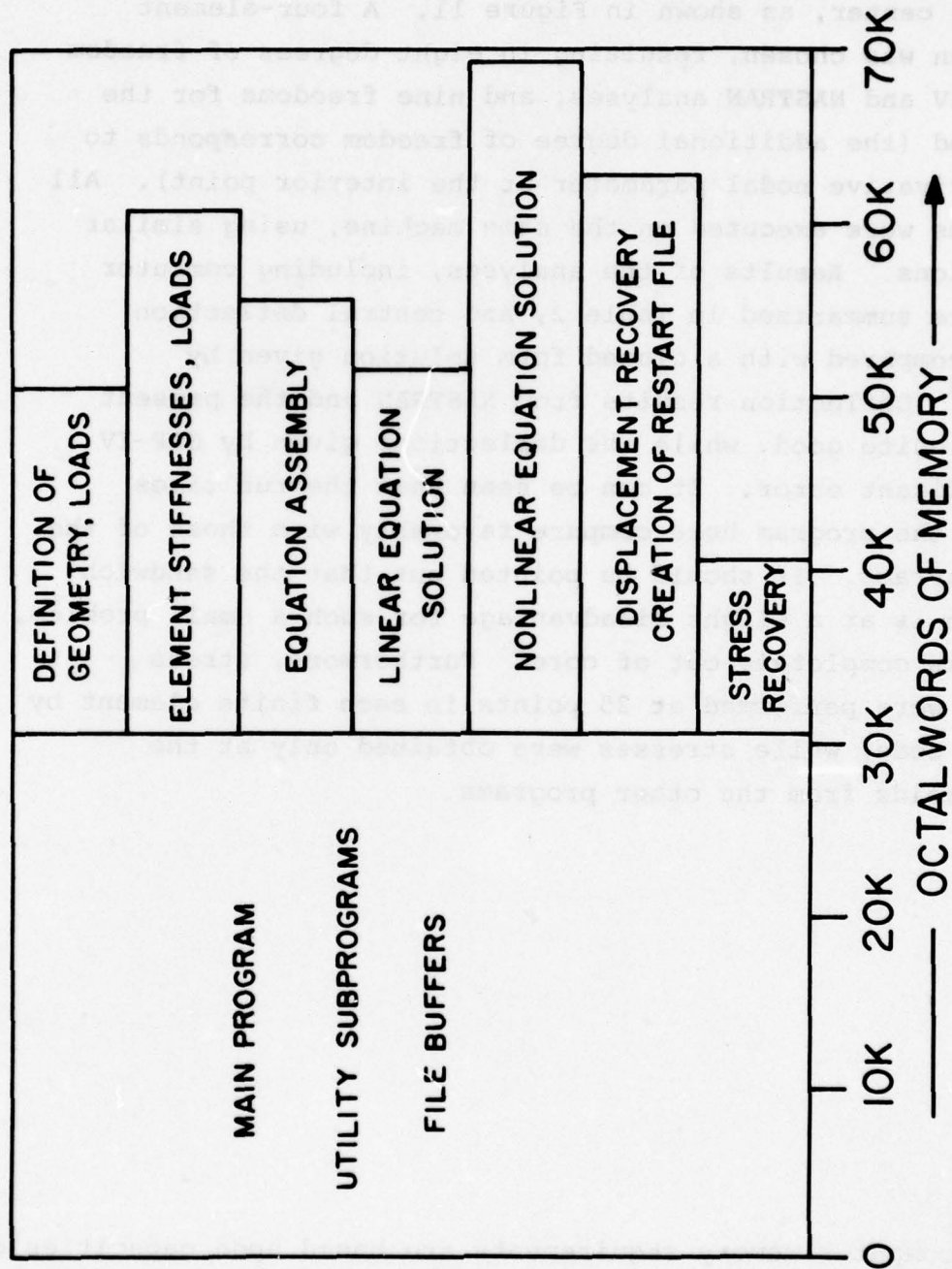


Figure 10. Computer Memory Requirements for Major Computer Program Segments (CDC 6600).

performed using only 62500 words of control memory.* To demonstrate the efficiency of the analysis program, the code has been tested on a small problem and compared with the general purpose programs SAP-IV²² and NASTRAN²³. The problem is that of a thin, flat plate loaded at the center, as shown in Figure 11. A four-element discretization was chosen, resulting in eight degrees of freedom for the SAP-IV and NASTRAN analyses, and nine freedoms for the present method (the additional degree of freedom corresponds to the cross-derivative nodal parameter at the interior point). All three programs were executed on the same machine, using similar compiler options. Results of the analyses, including computer run times, are summarized in Table 2, and central deflection results are compared with a closed form solution given by Timoshenko.²⁴ Deflection results from NASTRAN and the present analysis are quite good, while the deflections given by SAP-IV show a significant error. It can be seen that the run times required for the program here compare favorably with those of the other two programs. It should be pointed out that the sandwich computer code is at a slight disadvantage for such a small problem, since it works completely out of core. Furthermore, stress computations were performed at 25 points in each finite element by the sandwich code, while stresses were obtained only at the element centroids from the other programs.

* The above computer memory requirements are based upon capacities of 6000 degrees-of-freedom for the linear problem, and 1000 for nonlinear analysis, on a CDC 6600 machine.

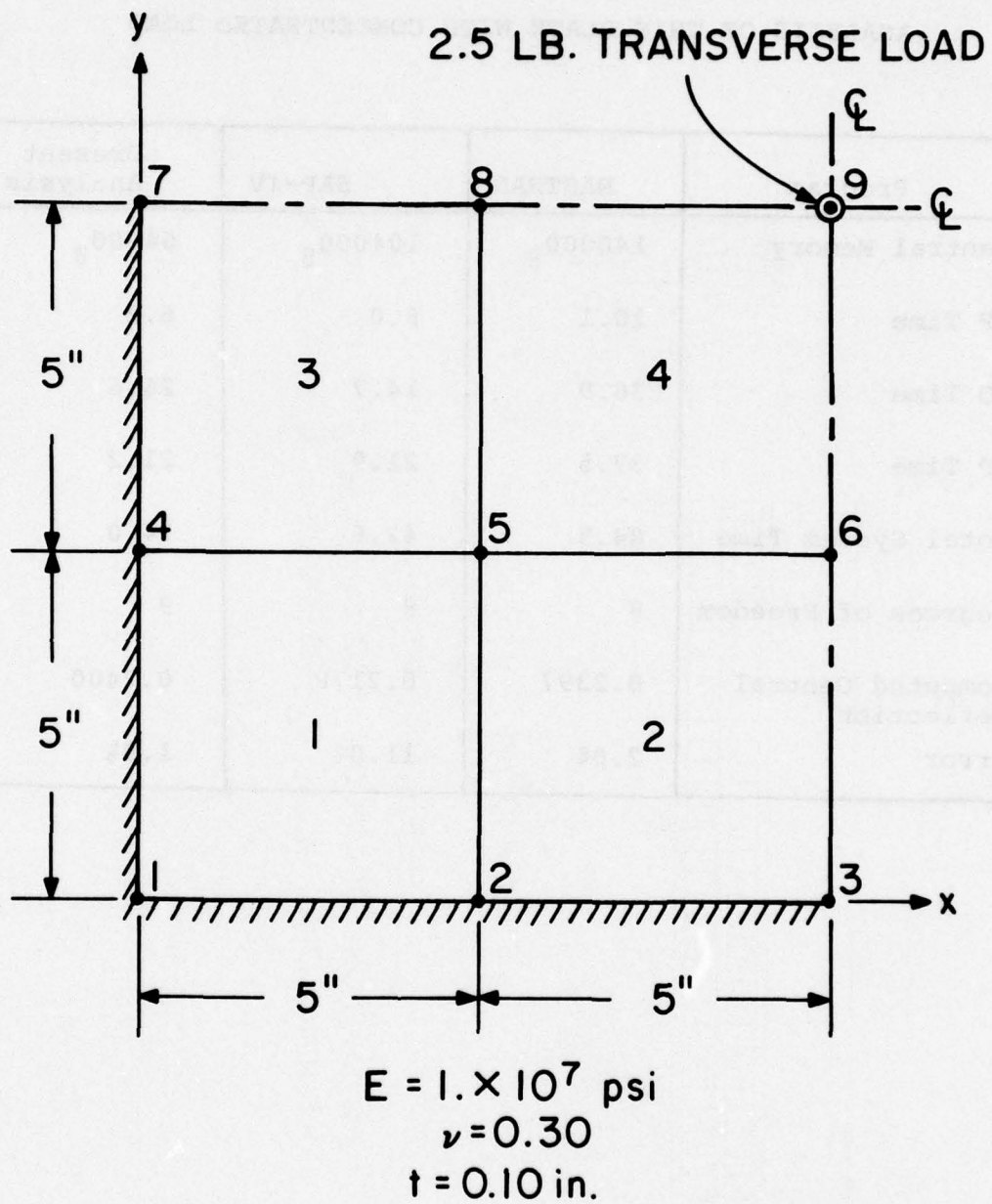


Figure 11. Flat Plate Problem for Computer Program Comparisons.

TABLE 2

RESULTS OF COMPUTER PROGRAM COMPARISON:
ANALYSIS OF THIN PLATE WITH CONCENTRATED LOAD

Program	NASTRAN	SAP-IV	Present Analysis
Central Memory	140000 ₈	104000 ₈	64000 ₈
CP Time	10.1	6.0	6.2
IO Time	36.9	14.7	26.6
PP Time	37.5	21.9	21.2
Total System Time	84.5	42.6	54.0
Degrees of Freedom	8	8	9
Computed Central Deflection	0.2397	0.2178	0.2400
Error	2.0%	11.0%	1.9%

SECTION 6

DEMONSTRATION PROBLEMS

Several numerical solutions based on the present analysis are presented in this section. Both linear and nonlinear problems are considered. Applications of the method to multicore sandwich constructions and nonrectangular panels are illustrated. It is shown that good accuracy is obtained for predictions of both displacement and stress response, even in the presence of geometric singularities.

6.1 Linear Analyses

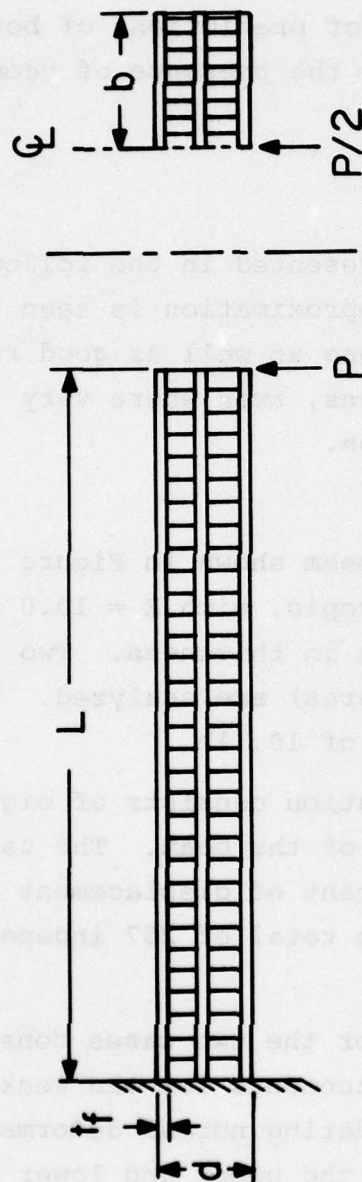
A number of linear analyses are presented in the following sections. The bicubic displacement approximation is seen to produce very smooth stress distributions as well as good representation of natural boundary conditions, even where very few elements are used in the discretization.

6.1.1 Multicore Sandwich Beam

The five-layer cantilever beam shown in Figure 12 is considered. All three faces are isotropic, with $E = 10.0 \times 10^6$ lb./in.², $\nu = 0.30$, and are 0.025 inch in thickness. Two sets of core properties (strong and weak cores) are analyzed. The beam is subjected to a transverse end load of 10. lb.

The finite element idealization consists of eight sandwich elements, four in each layer of the beam. The use of longitudinal symmetry and the enforcement of displacement continuity in the central layer results in a total of 237 independent degrees of freedom.

Calculated displacements for the two cases considered are listed in Table 3. The tip displacements for the weak-core case indicate the importance of considering normal deformations in the core layer; end deflections of the upper and lower faces are different by more than four percent in this example. Total



$E_f = 10.0 \times 10^6 \text{ psi}$ $L = 20.0 \text{ in.}$ $t_c = 0.25$
 $\nu_f = 0.30$ $d = 0.575 \text{ in.}$ $P/2 = 5.0 \text{ lbf.}$
 $t_f = 0.025 \text{ in.}$ $b = 5.0 \text{ in.}$
 WEAK CORE BEAM: $G_c = 1500. \text{ psi}$ $E_{zc} = 500. \text{ psi}$
 STRONG CORE BEAM: $G_c = 23500. \text{ psi}$ $E_{zc} = 10000. \text{ psi}$

Figure 12. Multicore Sandwich Beam.

TABLE 3

FREE END DISPLACEMENTS OF MULTICORE BEAMS

A. Weak Core Beam

	Displacement on Centerline	Displacement on Free Edge
Upper Face (Unloaded)	0.113	0.106
Central Face	0.114	0.106
Lower Face (Loaded)	0.118	0.108

B. Strong Core Beam

	Displacement on Centerline	Displacement on Free Edge
Upper Face (Unloaded)	0.0856	0.0839
Central Face	0.0856	0.0839
Lower Face (Loaded)	0.0858	0.0840

stresses in the lower sandwich face, along the centerline of the beam, are shown in Figure 13. Stress distributions for both beams are quite similar, except near the free end where high local face-bending stresses occur for the weak-core case. At the clamped edge, the total stresses are in agreement within three percent. The total moment developed at the root section is computed as 227. in.-lb., based on average membrane stresses in the two outermost faces. The actual moment due to the tip load at this section is 200. in.-lb., so that the natural boundary condition is well-represented despite the relative coarseness of the discretization. It should be mentioned that the above stresses have been computed along element edges, and that the values given for $x = 0., 5., 10.,$ and $20.$ are true nodal stress values, which are notorious in most finite element formulations for their sporadic behavior. The primary reason for the smoothness of the stress profiles in the present analysis is the enforcement of continuity of the membrane strains along interelement edges, made possible by the use of derivative-degrees of freedom. The differences between adjacent elements in total stresses, evaluated at the common nodes, are 0.15%, 0.80%, and 3.9% for the strong-core sandwich, and 4.6%, 5.2%, and 16% for the beam with a weaker core.

6.1.2 Skewed Sandwich Plate

A flat, rhombic sandwich plate having a skew angle of 45 degrees is analyzed for response to a pressure loading. Such a problem has been solved previously by finite elements²⁵ and by the Ritz method²⁶. The face sheets and core of the sandwich have the following properties:

$$\begin{array}{lll} E_f = 1. \times 10^7 \text{ lb./in.}^2 & \nu_f = 0.32 & t_f = 0.025 \text{ in.} \\ G_c = 500. \text{ lb./in.}^2 & t_c = 1.00 \text{ in.} & \end{array}$$

The transverse compression modulus of the core is taken to be very large, so that normal deformations in the core are suppressed. A uniform lateral pressure load of 1.0 lb./in.^2 is applied to the entire panel.

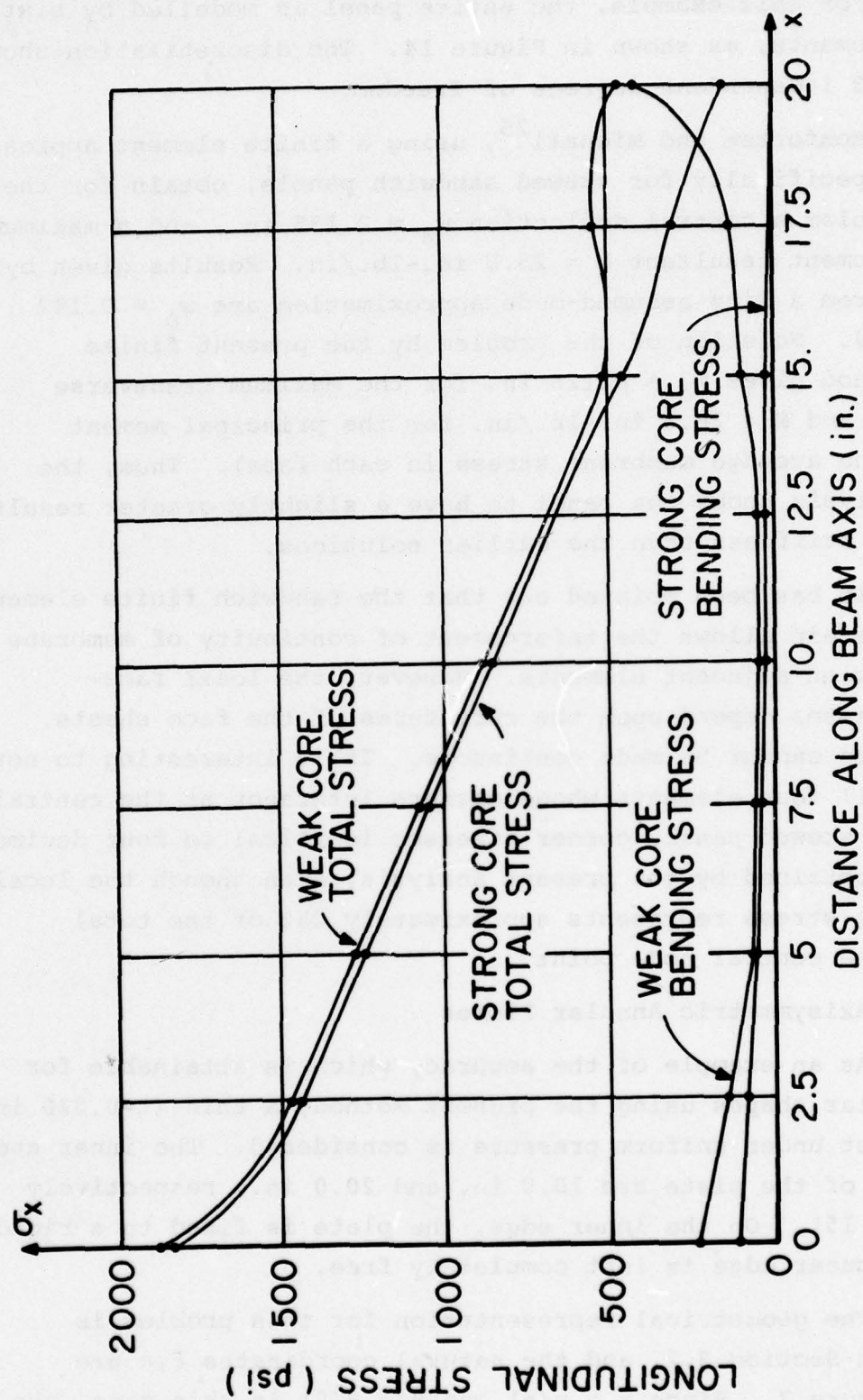


Figure 13. Lower Face Sheet Stress Distributions in Multicore Sandwich Beam.

For this example, the entire panel is modelled by sixteen sandwich elements, as shown in Figure 14. The discretization shown involved 328 independent degrees of freedom.

Monforton and Michail²⁵, using a finite element approach developed specifically for skewed sandwich panels, obtain for the present problem a central deflection $w_c = 0.135$ in., and a maximum principal moment resultant $M = 25.3$ in.-lb./in. Results given by Kennedy²⁶ from a Ritz assumed-mode approximation are $w_c = 0.142$ and $M = 25.4$. Solution of the problem by the present finite element method gives $w_c = 0.126$ in. for the maximum transverse deflection, and $M = 26.0$ in.-lb./in. for the principal moment (based on the average membrane stress in each face). Thus, the present analysis shows the panel to have a slightly greater resultant bending stiffness than the earlier solutions.

It has been pointed out that the sandwich finite element developed herein allows the enforcement of continuity of membrane strains between adjacent elements. However, the local face-bending stresses depend upon the curvatures of the face sheets, and therefore cannot be made continuous. It is interesting to note that, for all four elements whose corners intersect at the central node of the skewed panel, corner stresses identical to four decimal places are obtained by the present analysis, even though the local face-bending stress represents approximately 25% of the total stress at the central node point.

6.1.3 Axisymmetric Annular Plates

As an example of the accuracy which is attainable for nonrectangular shapes using the present method, a thin ($t=0.020$ in.) annular sheet under uniform pressure is considered. The inner and outer radii of the plate are 10.0 in. and 20.0 in., respectively (see Figure 15). On the inner edge, the plate is fixed to a rigid shaft. The outer edge is left completely free.

The geometrical representation for this problem is described in Section 3.2, and the natural coordinates ξ, η are shown in Figure 7. Since $r = r(\eta)$ and $\theta = \theta(\xi)$ in this case, the

$$E_f = 1. \times 10^7 \text{ psi}$$

$$\nu_f = 0.32$$

$$t_f = 0.025 \text{ in.}$$

$$G_c = 500. \text{ psi}$$

$$E_c = \infty$$

$$t_c = 1.00 \text{ in.}$$

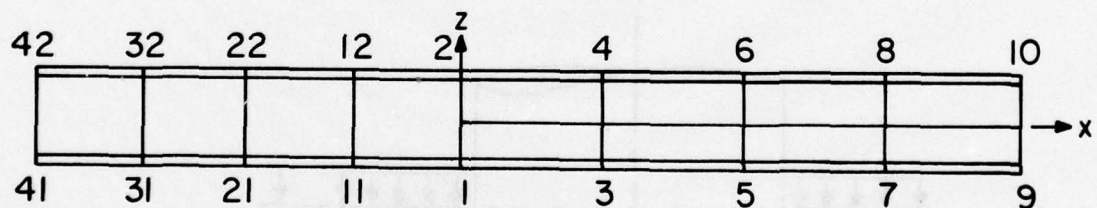
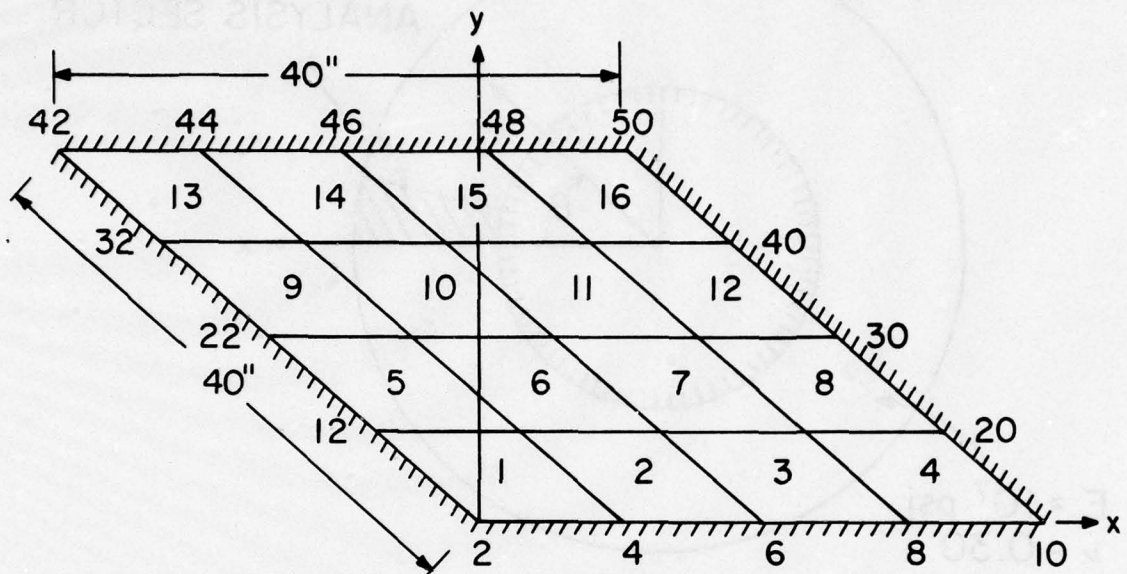


Figure 14. Skewed Sandwich Panel Discretization.

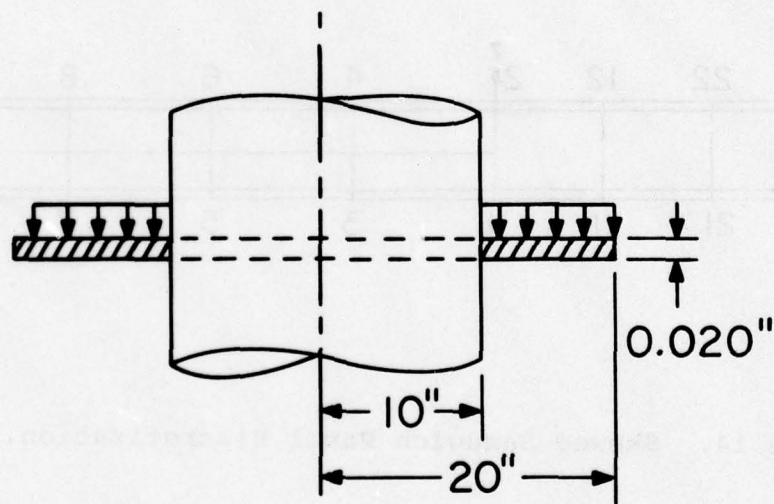
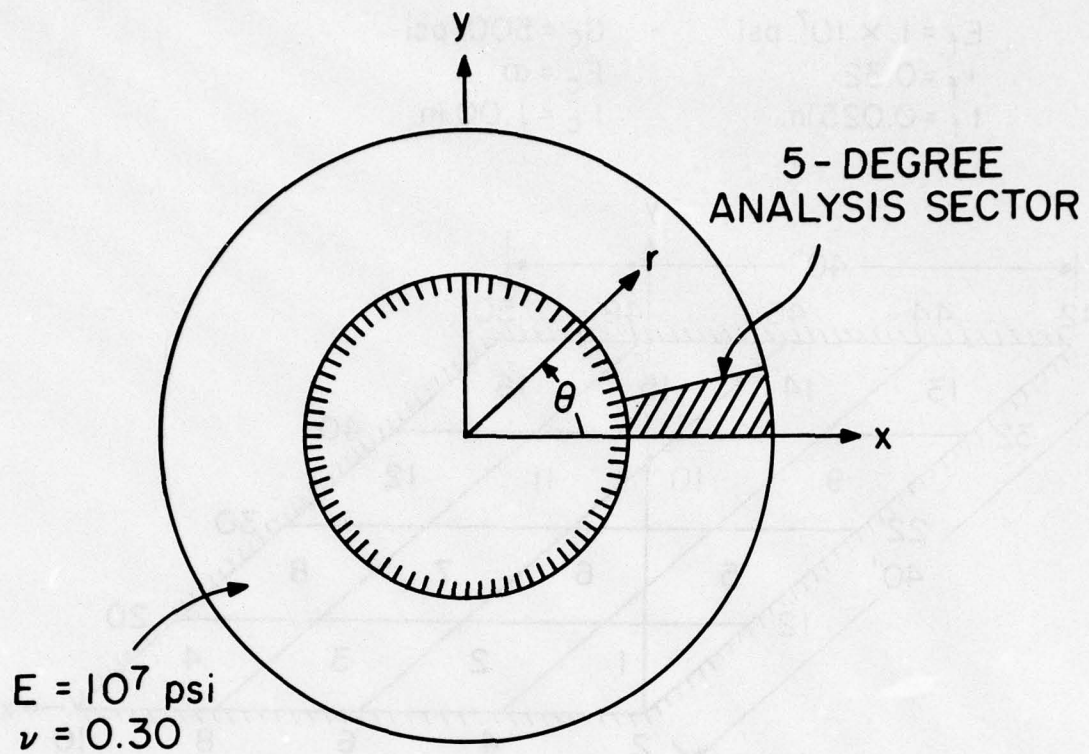


Figure 15. Thin Annular Sheet Geometry.

nodal parameters $w_{\xi ij}$ and $w_{\xi \eta ij}$ are zero due to the condition of zero tangential slope. The plate is modelled with a single finite element, resulting in a total of four unconstrained degrees of freedom. The nonzero nodal parameters correspond to w_{ij} and $w_{\eta ij}$ at each of the two nodes on the outer radius.

For a total load of 1 lb. ($p = 0.00106$ psi), the one-element solution yields a maximum deflection of $w_o = 0.1929$ inches, and a maximum radial stress of $\sigma_{ri} = 748.4$ psi at the support. An analytical solution given by Timoshenko²⁴ shows that $w_o = 0.1989$ and $\sigma_{ri} = 1102.4$ psi. The errors in transverse deflection and maximum stress are therefore 3.0 percent and 32.1 percent, respectively, for the numerical solution. This degree of accuracy, using only a single element, is quite good particularly when one notes that the average aspect ratio of the finite element used is slightly greater than nine to one.

The same problem (with $r_i = 5.0$ inches), has been solved using a 12 element discretization with 46 degrees of freedom. For this model, displacement results given by Timoshenko²⁴ are reproduced exactly, and the maximum stress at the clamped support is different from the analytical solution by 1.4 percent. The calculated stresses along a radial line are shown in Figure 16, normalized with respect to the maximum radial stress. As in the previous problem, a five degree sector of the plate is considered in the model, so that the average element aspect ratio is close to unity.

6.1.4 Circular Sandwich Panel

A uniformly loaded circular sandwich plate, shown in Figure 17, is considered. The face sheets are 0.025 in. aluminum, with $E_f = 10^7$ and $\nu_f = 0.30$. Properties of the core are $G_c = 26,000$ psi and $E_{cz} = 10^7$, with a thickness of 0.450 inches.

A previous finite element solution of this problem has been obtained by Sharifi²⁷, using eight axisymmetric sandwich elements in the radial direction. The discretization used here has three

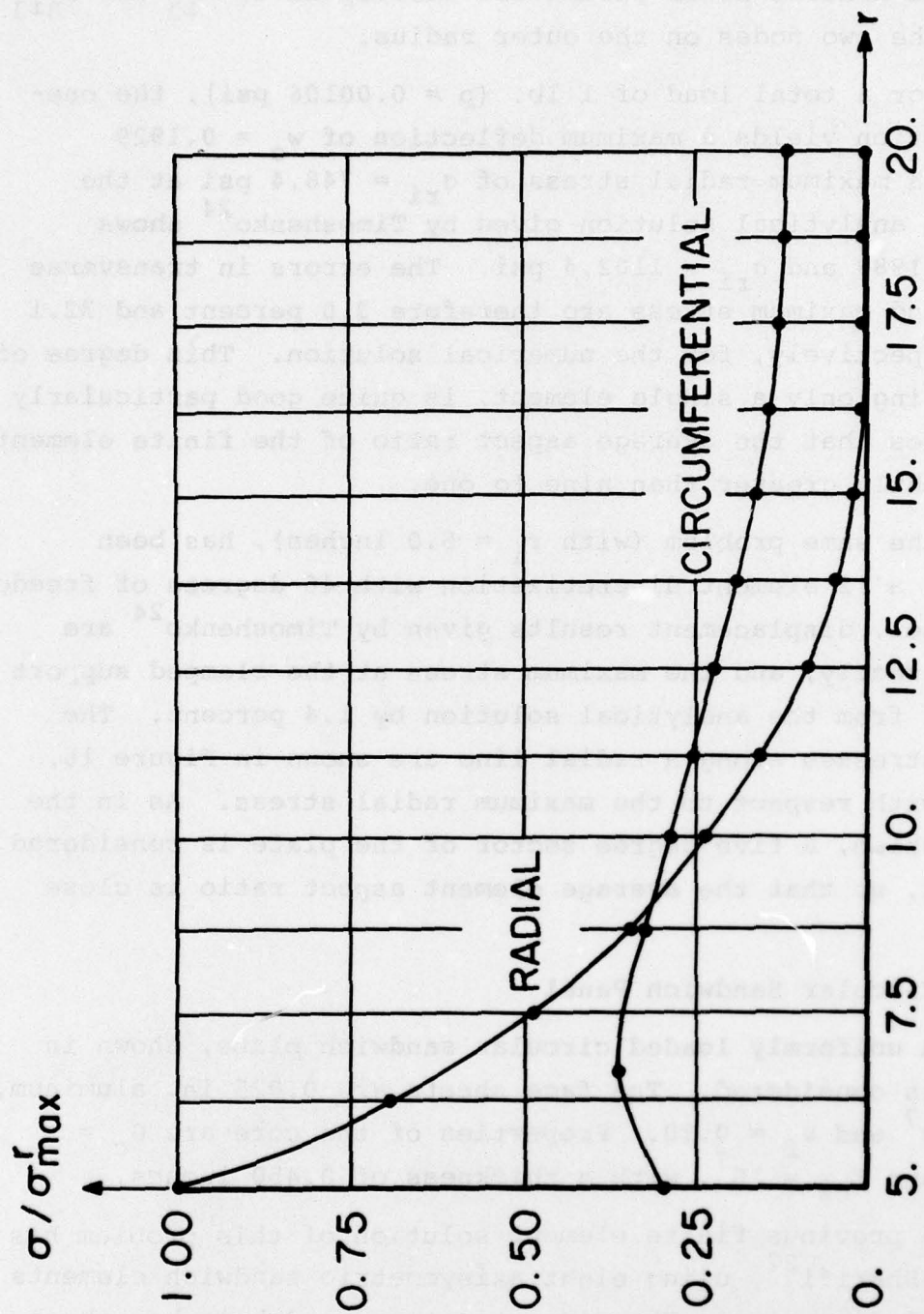


Figure 16. Computed Stress Distributions for Thin Annular Plate.

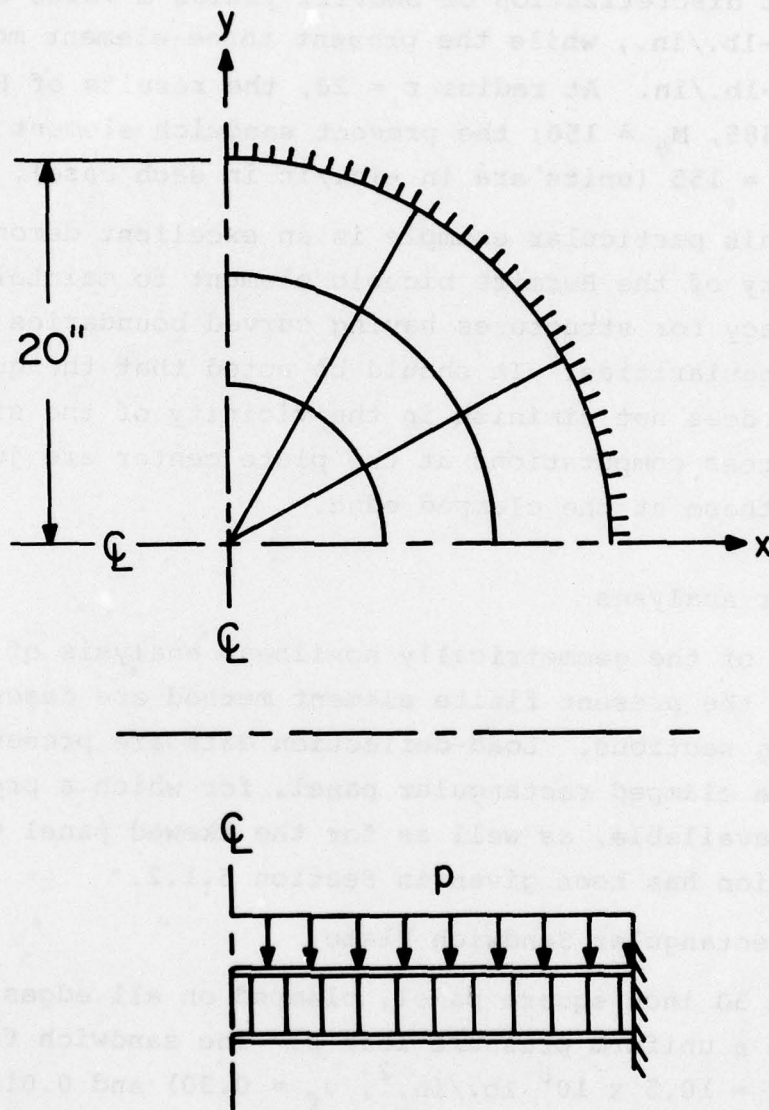


Figure 17. Circular Sandwich Panel Modelled with Degenerate Elements.

elements on the radius, with the innermost of these containing a geometric singularity where the element edge degenerates to a point.

Stress distributions for the lower face of the circular sandwich, shown in Figure 18, agree quite well with the results reported in Reference 27. For the central bending moment, the eight element discretization of Sharifi yields a value of $M \doteq -340$ in.-lb./in., while the present three-element model gives $M = -360$ in.-lb./in. At radius $r = 20$, the results of Reference 27 are $M_r \doteq 485$, $M_\theta \doteq 150$; the present sandwich element gives $M_r = 417$, $M_\theta = 155$ (units are in.-lb./in in each case).

This particular example is an excellent demonstration of the ability of the Hermite bicubic element to maintain good stress accuracy for structures having curved boundaries as well as geometric singularities. It should be noted that the quality of the solution does not diminish in the vicinity of the singularity, since the stress computations at the plate center are just as accurate as those at the clamped edge.

6.2 Nonlinear Analyses

Examples of the geometrically nonlinear analysis of sandwich plates using the present finite element method are described in the following sections. Load-deflection data are presented for the case of a clamped rectangular panel, for which a previous solution is available, as well as for the skewed panel whose linear solution has been given in Section 6.1.2.

6.2.1 Rectangular Sandwich Plate

A 50 inch square panel, clamped on all edges, is subjected to a uniform pressure load p . The sandwich faces are aluminum ($E_f = 10.5 \times 10^6$ lb./in.², $\nu_f = 0.30$) and 0.015 in. in thickness. The core layer is 1.0 in. thick and has shear modulus $G_c = 50000$ lb./in.²

The finite element model for this problem consists of four nonlinear sandwich elements, as shown in Figure 19. Due to the

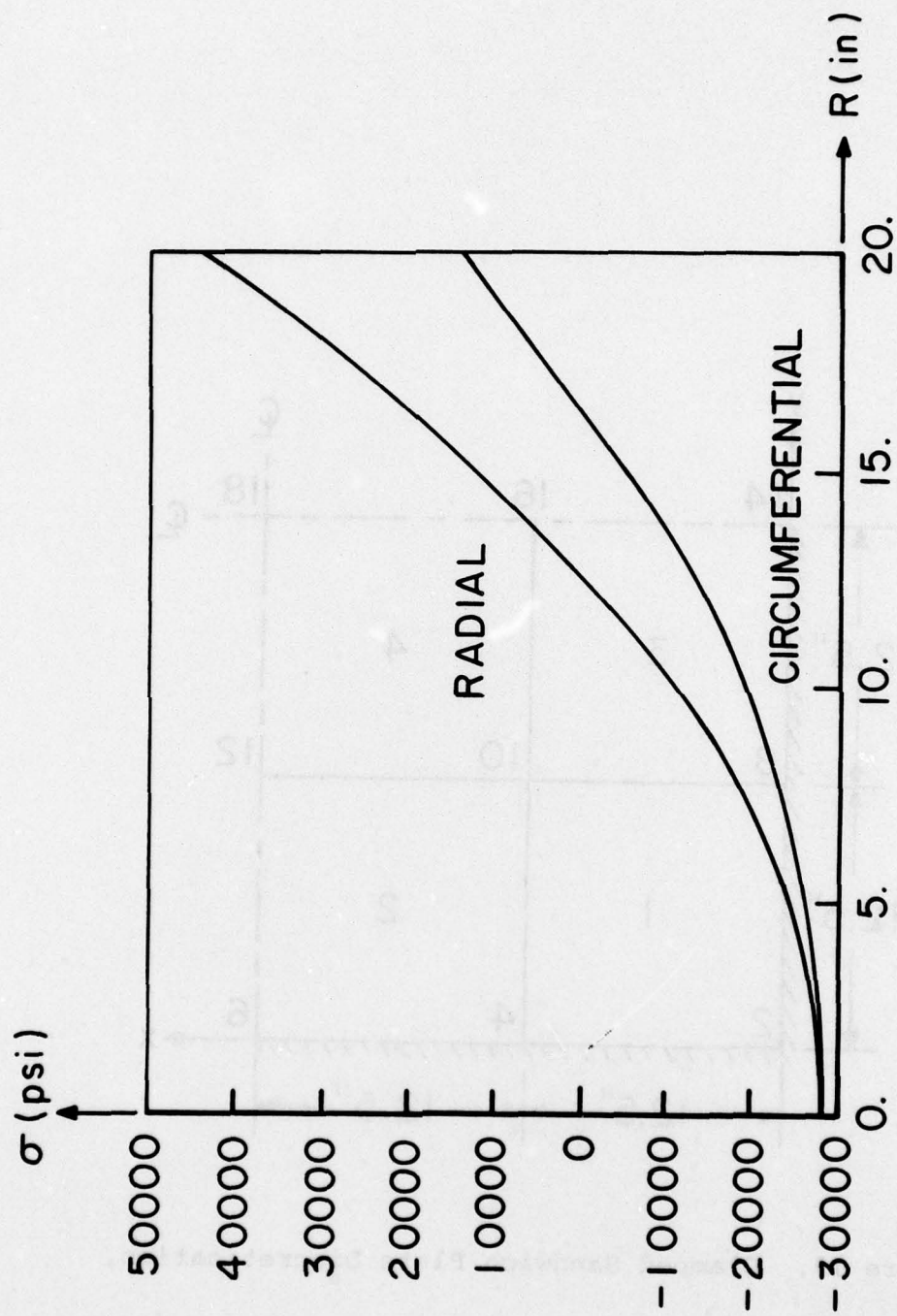


Figure 18. Lower Face Sheet Membrane Stress Distributions in Circular Sandwich Plate.

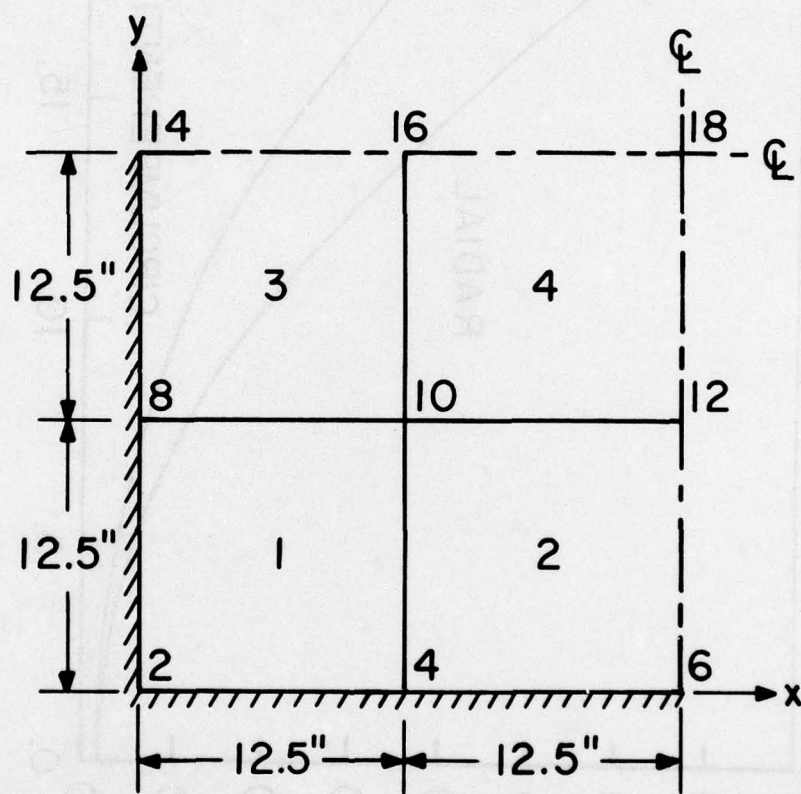


Figure 19. Clamped Sandwich Plate Discretization.

double symmetry of the problem, only one quadrant of the panel is considered; the resulting discretization has 120 independent degrees of freedom. Solutions for various values of the pressure loading are obtained using the variable-metric method of minimization (Section 4.3.1).

The load-deflection path for the present problem is shown in Figure 20 in terms of a central deflection ratio w_c/t_c and the loading parameter $Q = 12 \text{ pa}^3(1-\nu_f^2)/E_f t_f t_c^2$, where $2a = 50 \text{ in.}$ is the edge dimension of the panel. These results are compared with previous solutions given in References 3 and 28. The analysis presented in Reference 28 involves a perturbation solution for q in terms of the parameter w_c/t_c , and is limited to a two-term expansion of the form $Q = C_1(w_c/t_c) + C_2(w_c/t_c)^3$, where the ratio w_c/t_c is on the order of one. In Reference 3, a finite element solution is given, wherein it is assumed that the pressure loading acts at the midplane of the sandwich; such an assumption is necessary due to the neglect of normal deformations in the sandwich core. Antisymmetry conditions requiring that $u_1 = -u_2$, $v_1 = -v_2$ can then be imposed to reduce the number of degrees of freedom. It is more reasonable to suppose that the loading acts over one face of the panel, and this approach is taken in the present analysis. Figure 20 shows that the present method yields a solution which is slightly more flexible than that of the previous finite element analysis, and substantially more so than the perturbation solution of Reference 28.

The importance of a nonlinear analysis capability is evident from the load-deflection path for the present example. The deflection predicted, for example, at $Q = 30$. ($p = 27.7 \text{ psi}$) by the linear analysis is more than 55 percent greater than that obtained by taking geometric nonlinearities into consideration.

6.2.2 Skewed Sandwich Plate

The rhombic sandwich panel considered in Section 6.1.2 is reanalyzed, this time including the effects of geometric nonlinearities. A sixteen element model consisting of 328 independent

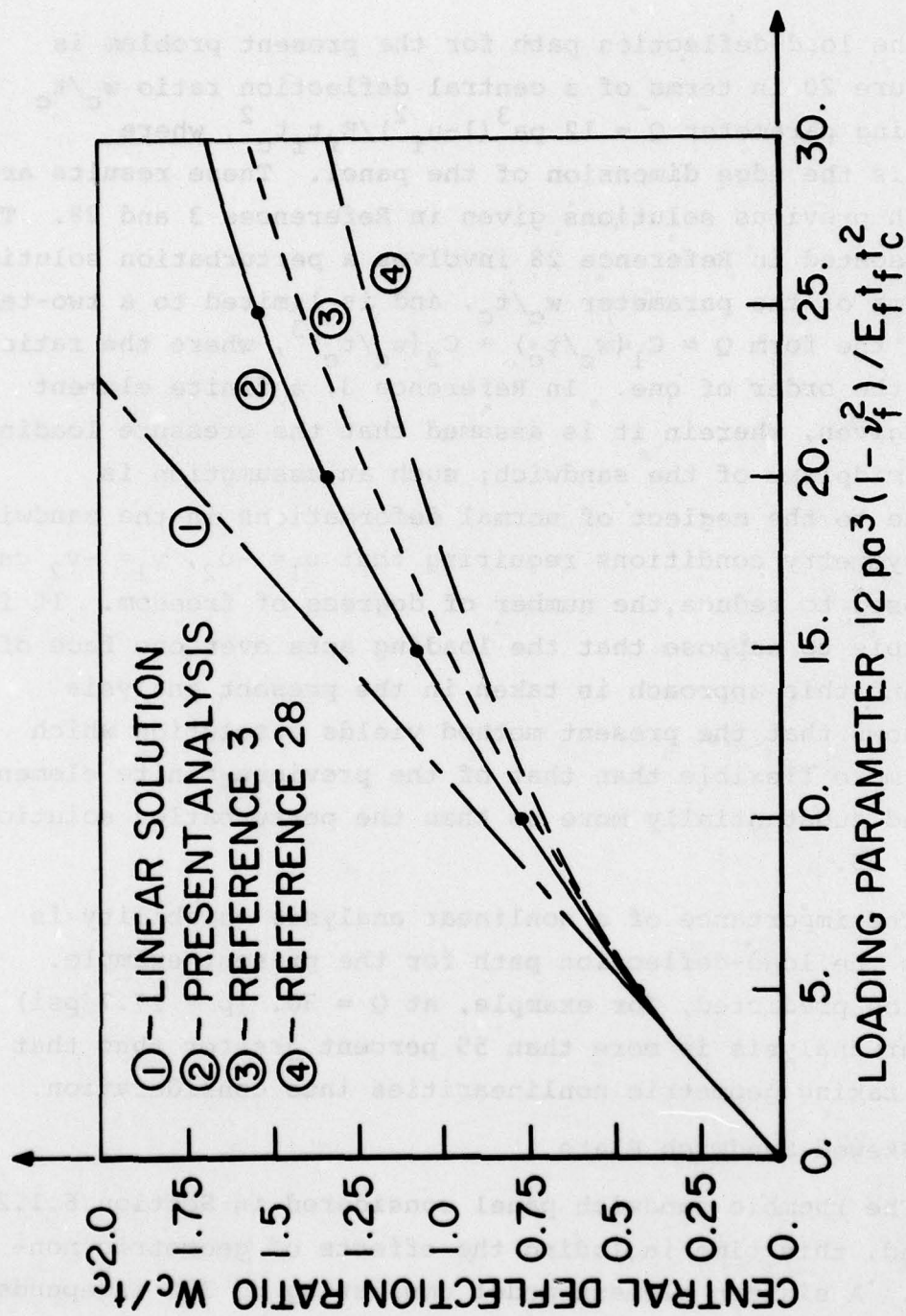


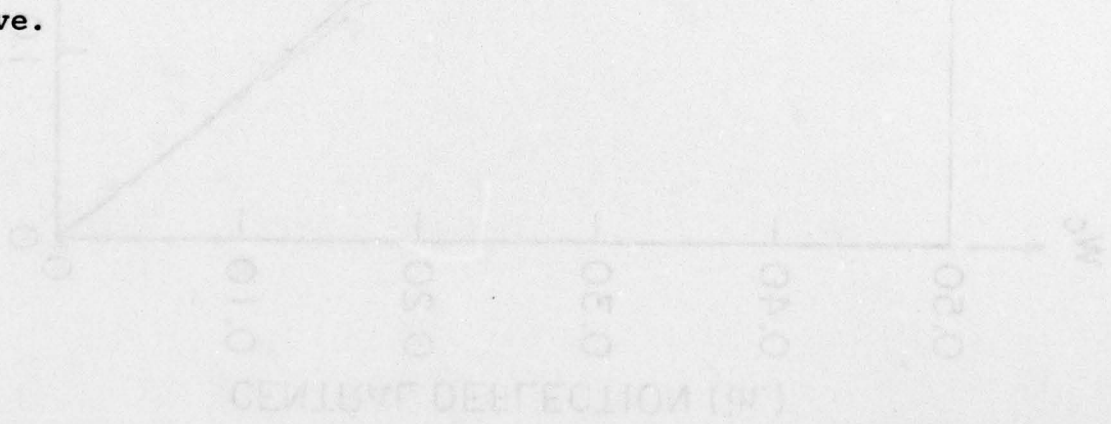
Figure 20. Load-Deflection Path for Clamped Sandwich Plate.

degrees of freedom is employed as the linear analysis. The Fletcher-Reeves method is used to obtain numerical solutions.

Load-deflection results for the skew panel are shown in Figure 21. Numerical solutions at pressures of 1.0, 2.5 and 5.0 psi are used to determine the curve, with the starting estimate for each solution vector extrapolated using all previous solutions. Although the Fletcher-Reeves iteration has been found to perform sluggishly at times on smaller problems (less than 100 degrees of freedom), its performance in the present problem is quite good. Using the linear solution at $p = 1.0$ psi as a starting point, the nonlinear iteration converges in only 17 iterations. The solutions for 2.5 psi and 5.0 psi are converged in 279 and 154 iterations, respectively, using a linear and then quadratic extrapolation for the starting vectors.

The effect of nonlinearity upon the response of the skew panel is a great deal more pronounced than for the square plate considered in the previous example. For the skew panel, the central deflection predicted by a linear analysis at a pressure of only 5.0 psi is more than 67% too large.

The importance of the computational procedure for the element potential energy and its gradient (Section 4.2) is evident, since more than two such evaluations, on the average, are necessary at each iteration in the minimization solution. For the present example, the average execution time per iteration is 1.38 seconds; thus, the method outlined in Section 4.2 is seen to be quite effective.



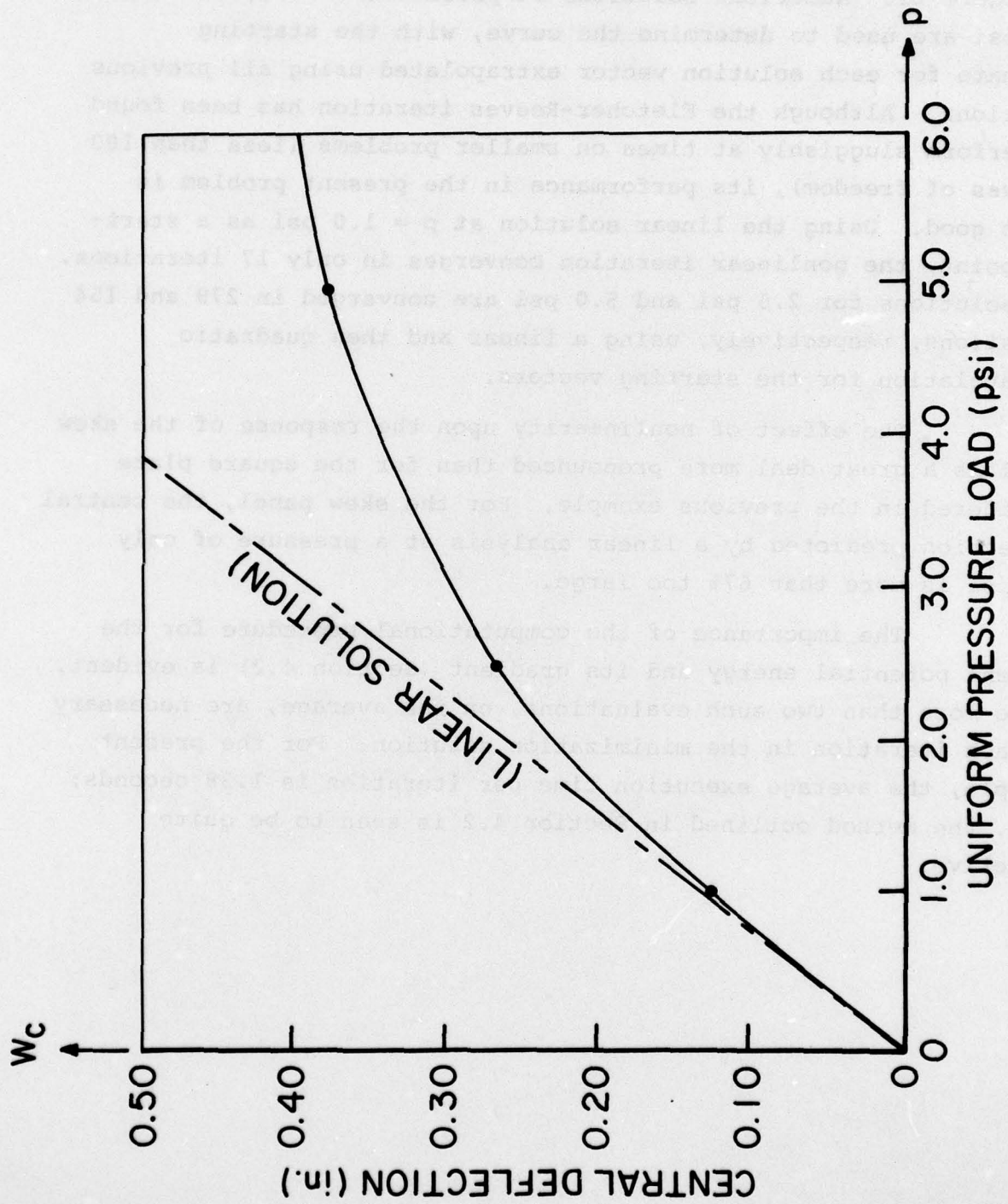


Figure 21. Central Deflection of Skewed Sandwich Panel.

SECTION 7

SUMMARY AND RECOMMENDATIONS

A parametric finite element formulation for the linear and geometrically nonlinear structural analysis of sandwich composite panels has been presented. The theoretical development includes effects due to local bending deformation in the sandwich faces, and both transverse shear and normal strains within the core layer. Use of the face sheet displacements as primary unknowns in the discretization permits the consideration of thin laminates, multicore sandwich, and "half-sandwich" constructions as well as the more common three-layer geometry. The discrete model is based upon Hermite bicubic interpolation in parametric coordinates, and is thus applicable to panels having curvilinear or skewed boundaries. Orthotropic material properties and effects due to membrane-bending stiffness coupling are also accounted for in the analysis. Displacement and stress results obtained using the parametric sandwich finite element are quite good, even on relatively coarse meshes, and solution accuracy is maintained even when modelling curvilinear shapes with degenerate elements.

The results summarized in this report represent a preliminary state of development of a more comprehensive sandwich composite analysis capability. The discrete formulation described, which is capable of considering a fairly general class of undeformed panel geometries, can be extended to model sandwich shell geometry as well as multiple plate or shell constructions joined at arbitrary angles. Provisions for including stiffening members and attachments to surrounding structure are important as well, but were not implemented in the present effort. Future extensions to the present analysis should also include consideration of material non-linearity, and dynamic as well as static structural response.

The research described herein suggests that refined finite element approximations such as the parametric bicubic can be successfully adapted to the general nonlinear analysis of structures

of a practical nature. Although the element formulation is relatively complex, the resulting numerical performance is extremely good. Computational requirements are generally modest due to the high solution accuracy which is attained on relatively coarse grids.

REFERENCES

1. Reissner, E., "Finite Deflections of Sandwich Plates," *Journal of the Aeronautical Sciences*, Vol. 15, No. 7, July 1948.
2. Brockman, R.A., "Buckling of Cylindrical Sandwich Panels with Laminated Faces," AFFDL-TR-76-151, January 1977.
3. Monforton, G.R., "Discrete Element, Finite Displacement Analysis of Anisotropic Sandwich Shells," Report No. 39, Division of Solid Mechanics, Structures and Mechanical Design, School of Engineering, Case Western Reserve University, January 1970.
4. Novozhilov, V.V., Foundations of the Nonlinear Theory of Elasticity, Graylock Press, Rochester, N.Y., 1953.
5. Ashton, J.E., J. C. Halpin and P. H. Petit, Primer on Composite Materials: Analysis, Technomic Publ. Co., Stamford, Conn., 1969.
6. Washizu, K., Variational Methods in Elasticity and Plasticity, Pergamon Press, 1968.
7. Strang, G. and G. J. Fix, An Analysis of the Finite Element Method, Prentice-Hall, Inc., Englewood Cliffs, N.J., 1973.
8. Bogner, F. K., R. L. Fox and L. A. Schmit, "The Generation of Interelement-Compatible Stiffness and Mass Matrices by the use of Interpolation Formulas," *Proceedings of the Conference on Matrix Methods in Structural Mechanics*, Wright-Patterson Air Force Base, Ohio, 1966.
9. Hildebrand, F. B., Introduction to Numerical Analysis, McGraw-Hill Co., New York, 1956.
10. Palacol, E. L. and E. L. Stanton, "Anisotropic Parametric Plate Discrete Elements," International Journal for Numerical Methods in Engineering, Vol. 6, pp. 413-425, 1973.

REFERENCES, continued

11. Bogner, F. K., "Finite Deflection, Discrete Element Analysis of Shells," Report No. 5, Division of Solid Mechanics, Structures and Mechanical Design, Case Western Reserve University, August 1967.
12. Coons, S. A., "Surfaces for Computer-Aided Design of Space Figures," M.I.T. Preprint No. 299, January 1964.
13. Bathe, K. J. and E. L. Wilson, Numerical Methods in Finite Element Analysis, Prentice-Hall, Inc., Englewood Cliffs, N.J., 1976.
14. Zienkiewicz, O. C., The Finite Element Method in Engineering Science, McGraw Hill Co., London, 1971.
15. Schmit, L. A., F. K. Bogner and R. L. Fox, "Finite Deflection Structural Analysis Using Plate and Shell Discrete Elements," AIAA Journal, Vol. 6, No. 5, 1968.
16. Schmit, L. A., et al., "Developments in Discrete Element Finite Deflection Structural Analysis by Function Minimization," AFFDL-TR-68-126, September 1968.
17. Davidon, W. C., "Variable Metric Method for Minimization," ANL-5990 Rev., University of Chicago, 1959.
18. Fletcher, R. and M. J. D. Powell, "A Rapidly Convergent Descent Method for Minimization," Computer Journal, Vol. 6, No. 2, 1963.
19. Fletcher, R. and C. M. Reeves, "Function Minimization by Conjugate Gradients," Computer Journal, Vol. 7, No. 2, 1964.
20. Fox, R. L., Optimization Methods for Engineering Design, Addison-Wesley Publishing Co., Menlo Park, Calif., 1973.
21. Control Data Corporation, Loader Reference Manual (6000 Series), Publication No. 60344200, 1975.

REFERENCES, concluded

22. Bathe, K. J., E. L. Wilson and F. E. Peterson, SAP-IV: A Structural Analysis Program for Static and Dynamic Response of Linear Systems, Report No. EERC 73-11, College of Engineering, University of California, Berkeley, June 1973.
23. _____, The NASTRAN User's Manual (Level 16.0), NASA SP-222 (03), Scientific and Technical Information Office, National Aeronautics and Space Administration, Washington, D.C., March 1976.
24. Timoshenko, S. P., Theory of Plates and Shells, McGraw Hill Co., New York, 1959.
25. Monforton, G. R. and M. G. Michail, "Finite Element Analysis of Skew Sandwich Plates," Proceedings of the ASCE, Journal of the Engineering Mechanics Division, Vol. 98, No. EM3, 1972.
26. Kennedy, J. B., "On the Deformation of Parallelogrammic Sandwich Panels," The Aeronautical Journal, Royal Aeronautical Society, June 1970.
27. Sharifi, P., "Nonlinear Analysis of Sandwich Structures," Ph.D. Thesis, University of California, Berkeley, 1970.
28. Kan, H. P. and J. C. Huang, "Large Deflection of Rectangular Sandwich Plates," AIAA Journal, Vol. 5, No. 9, 1967.